ADVANCING EARTH AND SPACE SCIENCES

Earth and Space Science

RESEARCH ARTICLE

10.1029/2022EA002649

Key Points:

- Solar Occultation for Ice Experiment (SOFIE) ozone (O_3) is within the uncertainties of other data sets between ~30 and 70 km altitude
- SOFIE O_3 is biased 5%–10% low above 70 km and below 30 km
- Higher mean difference values above 70 km occur due to low O_3 concentrations, limited coincidences, and large data uncertainties

Correspondence to:

S. Das,
saswad1@vt.edu

Citation:

Das, S., Bailey, S. M., Hervig, M. E., Thurairajah, B., & Marshall, B. T. (2023). Validation of version 1.3 ozone measured by the SOFIE instrument. *Earth and Space Science*, *10*, e2022EA002649. https://doi.org/10.1029/2022EA002649

Received 19 OCT 2022
Accepted 15 SEP 2023

Author Contributions:

Conceptualization: S. Das
Data curation: S. Das, M. E. Hervig, B. T. Marshall
Formal analysis: S. Das, S. M. Bailey, M. E. Hervig, B. Thurairajah
Funding acquisition: S. M. Bailey
Investigation: S. Das
Methodology: S. Das
Project Administration: S. M. Bailey
Resources: S. Das, M. E. Hervig, B. T. Marshall
Supervision: S. M. Bailey, B. Thurairajah
Validation: S. Das, M. E. Hervig, B. T. Marshall
Visualization: S. Das, S. M. Bailey, B. Thurairajah
Writing – original draft: S. Das

Validation of Version 1.3 Ozone Measured by the SOFIE Instrument

S. Das[1], S. M. Bailey[1], M. E. Hervig[2], B. Thurairajah[1], and B. T. Marshall[3]

[1]Bradley Department of Electrical and Computer Engineering, Center for Space Science and Engineering Research, Blacksburg, VA, USA, [2]GATS Inc, Driggs, ID, USA, [3]GATS, Inc., Newport News, VA, USA

Abstract The Solar Occultation for Ice Experiment (SOFIE) has operated aboard the Aeronomy of Ice in the Mesosphere (AIM) satellite since 2007. SOFIE uses solar occultation to retrieve ozone (O_3) profiles from ~20 to 100 km altitude, typically at polar latitudes. This study validates SOFIE O_3 profiles, including error analysis and comparisons with independent observations. Comparisons are made to the Atmospheric Chemistry Experiment Fourier Transform Spectrometer (ACE-FTS) and the Michelson Interferometer for Passive Atmospheric Sounding (MIPAS) satellite instruments. SOFIE shows qualitative and quantitative agreement with both data sets between 30 and 70 km and better overall agreement in the northern hemisphere. SOFIE and ACE mean differences are typically within 20% in the 30–70 km altitude range. SOFIE and MIPAS exhibit mean difference values within 30% in the winter and 20% for all other seasons averaged, between ~30 and 60 km. Seasonal comparisons indicate similar variations in both hemispheres and through all seasons. The comparisons indicate that SOFIE is biased 5%–10% low at 30–70 km altitudes, with greater differences at higher and lower altitudes. The comparisons are challenging due to the low O_3 concentrations at high altitudes, the limited number of coincidences, and the large diurnal variation in mesospheric O_3 during twilight hours.

Plain Language Summary Ozone is an important species in the middle atmosphere that requires continuous and high-quality measurements. Novel measurements from new satellite instruments are important to this end. The Solar Occultation for Ice Experiment (SOFIE) instrument measures the solar energy passing through the limb of the Earth's atmosphere at sunrise and sunset (relative to the spacecraft) that is used for retrieving ozone profiles. The profiles are compared to coincident profiles from other satellite instruments during winter and non-winter months in both hemispheres. The agreement between SOFIE and the data sets is considered reasonable when the mean difference is less than 30%. SOFIE agrees best with the other data sets in the 30–70 km altitude range. At high altitudes, low O_3 concentration, the limited number of coincidences between SOFIE and other data sets, and the large diurnal mesospheric O_3 variability during twilight make it difficult to compare SOFIE with other data sets.

1. Introduction

Ozone (O_3) is an important molecule in the middle atmosphere due to its ability to absorb solar ultraviolet (UV) radiation. The primary O_3 maximum lies in the stratosphere's ~25–40 km altitude range (McCormick et al., 1989). While the seasonal variability of O_3 concentration depends on the seasonal variation in temperature in the upper stratosphere (~40–50 km), photochemistry is much slower in the lower stratosphere (~25–40 km) due to the reduced UV flux. Thus, the transport of O_3 is attributed to atmospheric circulation, which drives the seasonal variation of O_3. The primary circulation is upwards in the tropics and poleward/downward in the mid and high latitudes in the lower stratosphere (Levy et al., 1985; Randel et al., 2008). The dissipation of wave disturbances propagated from the troposphere drives the circulation. During the winter, the dissipation of these waves in the stratosphere leads to downward/poleward circulation. The circulation carries O_3 produced at tropical source regions to high latitudes (Perliski et al., 1989; Solomon et al., 1985). During the winter, stratospheric O_3 is shielded from UV radiation by the O_3 above. Additionally, the solar zenith angle is high in the high latitude winter. This results in weaker photochemical O_3 loss. The accumulation of O_3 over the winter results in a springtime maximum. The local solar zenith angle is smaller in the summer, leading to efficient photochemistry. This leads to photochemical loss of O_3 over the summer, and a minimum is attained in late autumn (Stolarski et al., 1991, 1992).

Writing – review & editing: S. M. Bailey, B. Thurairajah

Besides its ability to shield us from harmful UV radiations that reach the surface of the Earth, O_3 plays an important role in regulating climate (Kuttippurath et al., 2021; Riese et al., 2012). Changes in the stratospheric O_3 have a large impact on the climate. Due to the emission of O_3-depleting substances, particularly Chlorofluorocarbons (CFCs), a decline in polar O_3 became evident over Antarctica by the late 1970s (Chubachi, 1984; Farman et al., 1985). Salby et al. (2011), Kuttippurath et al. (2013), Solomon et al. (2016), and Chipperfield et al. (2017) demonstrated the effectiveness of the Montreal Protocol in reducing halogen gases in the atmosphere, thus, corresponding to a positive trend in Antarctic O_3. The Montreal Protocol, its amendments and adjustments have efficiently decreased the abundance of ozone-depleting substances (ODSs) (WMO, 2022). O_3 recovery is most clearly observed in the upper stratosphere and Antarctic lower stratosphere in the spring. Due to large natural variability and factors such as climate change and tropospheric O_3 variability, the recovery of O_3 associated with ODs is difficult to detect. Further, an Arctic O_3 trend is difficult to detect compared to the Antarctic (Solomon et al., 2014) due to the relatively large variability. New results since the 2018 Assessment (WMO, 2018) suggest that the recovery of the Antarctic stratospheric O_3 continues to progress, and the O_3 hole has generally diminished in size since 2000. Further, the Antarctic O_3 holes observed in 2019 and 2020 showed significant variability in size, strength, and longevity and are largely dynamically driven. Observed O_3 trends in the Arctic remain small compared to the large interannual variability (precluding the identification of statistically significant O_3 in the Arctic between 2000 and 2021), with the Arctic total O_3 reaching exceptionally small values in spring 2020 (WMO, 2022). Cold Antarctic winters with very low stratospheric temperatures and a strong vortex that showed relatively large O_3 losses were reported in 1996, 2000, 2003, 2006, and 2015 (Bodeker et al., 2005; Chipperfield et al., 2017). Smaller O_3 holes were reported in 1998, 2002, 2012, and 2019 that had warmer winters, where the relatively higher temperatures led to the evaporation of Polar Stratospheric Clouds (PSCs) that provided their surfaces to halogen reservoirs species for conversion into O_3-destroying reactive forms (De Laat & Van Weele, 2011; Kuttippurath et al., 2015; Müller et al., 2008; Safieddine et al., 2020). Sinnhuber et al. (2000), Chipperfield et al. (2005), and von der Gathen et al. (2021) suggested that cold winters would get colder with increasing O_3 loss. Therefore, extremely large O_3 loss during cold winters could be a strong indicator of climate change, necessitating continuous O_3 measurements at high latitudes and over the polar vortex, particularly during the winter and spring. However, these levels do not contribute significantly to the total O_3 column changes discussed earlier.

O_3 is abundantly present in a layer in the upper mesosphere and lower thermosphere, known as the secondary O_3 maximum. The altitude of the secondary O_3 maximum in terms of mixing ratios lies between 90 and 92 km during daytime. While the nighttime O_3 mixing ratios in the secondary maximum region are comparable to what is found in the stratospheric maximum (~10 ppm), the daytime mixing ratios are relatively smaller but significantly larger than in the middle and upper mesosphere (Smith et al., 2008, 2009, 2011, 2013; Smith and Marsh., 2005; Tweedy et al., 2013).

In the stratosphere, O_3 impacts the stratospheric radiative balance. In the upper mesosphere and lower thermosphere, the secondary O_3 maximum (Smith and Marsh, 2005; Smith et al., 2009) is highly variable and, thus, difficult to characterize accurately. Thus, the stratosphere, upper mesosphere, and lower thermosphere are important atmospheric O_3 reservoirs, making it important to have continuous, high-quality O_3 measurements in these atmospheric regions (Cracknell & Varotsos, 2012; Smith et al., 2013). Solar occultation measurements are advantageous due to the high signal-to-noise ratio, allowing increased vertical and spectral resolution measurement at higher altitudes. Moreover, solar occultation measurements generally suffer less significant non-LTE effects and are self-calibrating by taking the ratio of the radiances (Dupuy et al., 2009).

The Solar Occultation for Ice Experiment (SOFIE) has operated onboard the Aeronomy of Ice in the Mesosphere (AIM) spacecraft since 2007 (Russell et al., 2009). SOFIE makes daytime measurements using solar occultation during sunrise and sunset relative to the spacecraft. SOFIE (Gordley et al., 2009a, 2009b) has a vertical resolution of ~1.8 km and typically observes high latitudes (65°–85°) in both hemispheres. The detailed SOFIE measurement approach is discussed in Section 2.1. Past satellite instruments have measured O_3 in the stratosphere, mesosphere, and lower thermosphere. These include SAGE II (the Stratospheric Aerosol and Gas Experiment) (Cunnold et al., 1989; Mauldin III et al., 1985; McCormick, 1987), SAGE III (SAGE ATBD Team, 2002), the HALogen Occultation Experiment (HALOE) (Russell et al., 1993), the Polar Ozone and Aerosol Measurement (POAM) III (Lucke et al., 1999), the SCanning Imaging Absorption spectroMeter for Atmospheric CHartographY (SCIAMACHY) (Bovensmann et al., 1999) and the Michelson Interferometer for Passive Atmospheric Sounding (MIPAS) (Fischer et al., 2008). Current satellite O_3 measurements are from the Atmospheric Chemistry

Experiment–Fourier Transform Spectrometer (ACE-FTS) (Bernath, 2001; Bernath et al., 2005), Sounding of the Atmosphere using Broadband Emission Radiometry (SABER) (Russell et al., 1999), SAGE III on the International Space Station (ISS) (Bognar et al., 2022; Cisewski et al., 2014; McCormick et al., 2020), Microwave Limb Sounder (MLS) (Jiang et al., 2007; Waters et al., 2006), Ozone Mapping and Profiler Suite (OMPS) (Flynn et al., 2006, 2014; Kramarova et al., 2014), and Optical Spectrograph and Infrared Imager System (OSIRIS) (Adams et al., 2012, 2014; Bourassa et al., 2018) instruments. SOFIE provides measurements from ~20 to 100 km altitude covering 15+ years, making an important addition to the O_3 record. Additionally, SOFIE's ability to continuously measure at high latitudes makes it an important instrument in studying O_3 loss and recovery within the polar vortex during winter and spring.

This paper validates the current publicly available SOFIE O_3 measurements (version 1.3) using error analysis and comparisons with ACE-FTS and MIPAS observations. Section 2 describes the SOFIE O_3 measurement approach, retrieval method, and uncertainty analysis. The correlative data sets are described in Section 3. The comparisons with ACE and MIPAS are presented in Section 4, and the impact of O_3 diurnal variability on the results is discussed in Section 5. The summary and conclusions of this study are presented in Section 6.

2. SOFIE O_3 Measurement Approach, Retrieval, and Uncertainty Analysis

2.1. SOFIE Measurement Approach

SOFIE measurements at 16 wavelengths (0.29–5.32 μm) are used to retrieve vertical profiles of temperature, five gaseous species (O_3, H_2O, CO_2, CH_4, and NO), polar mesospheric cloud (PMC) extinction, and meteoric smoke extinction (Gordley et al., 2009a, 2009b; Hervig et al., 2009a, 2009b; Marshal et al., 2011). Solar occultation measures solar intensity as rays pass through the atmosphere during spacecraft sunrise or sunset. Atmospheric transmission (T) is determined from the ratio of the atmospheric signal (V) over that measured above the atmosphere (V_O), $T = V/V_O$, which is then used to retrieve the geophysical parameters of interest. Because solar occultation does not require an absolute response calibration, it is immune to many error sources that are typical in other approaches. During 2007–2017, spacecraft sunset and sunrise measurements occurred in the Southern Hemisphere (SH) and Northern Hemisphere (NH), respectively. This switched in late 2018 due to the changing AIM orbit, with sunset (sunrise) measurements occurring in the NH (SH). This work uses SOFIE V1.3 data, which is available online (sofie.gats-inc.com).

2.2. SOFIE O_3 Retrieval

This study uses data from SOFIE Level 2 processing, which retrieves individual profiles of trace species, temperature, and aerosol extinction from the signals (Gordley et al., 2009a, 2009b). The retrievals rely on signal simulations that describe the radiative transfer of sunlight through Earth's atmosphere and account for the effects of the instrument. Line-by-line radiative transfer calculations with necessary line parameters (Gordley et al., 1994), assuming a spherically symmetric atmosphere, are used to simulate atmospheric transmissions. An "onion-peeling" (Russell & Drayson, 1972) technique is implemented to retrieve the limb profiles. The volume mixing ratio (VMR) of the target species is inferred in a top-down approach, with the VMR of the target species adjusted until the measured transmission is reproduced to within the noise. SOFIE measurements are over-sampled at 20 Hz, which corresponds to ~0.2 km vertical spacing at the tangent point. The SOFIE approach separates each profile into seven separate profiles with 1.4 km spacing, which is close to the native vertical resolution (~1.6 km). These profiles are used for independent retrievals, which are then combined with a 0.7 km Gaussian filter to decrease random errors. The resulting final profile is reported on the original 0.2 km vertical grid.

O_3 is measured using two broadband (~2% filter width) filters centered at 292 and 330 nm wavelength (Bands 1 and 2, respectively), as shown in Figure 1. Note that the Band 2 electronic response was saturated at launch but came into range by November 2009 due to the normal darkening of the UV optics over time (Gordley et al., 2009a, 2009b). From launch until November 2009, O_3 was not reported below ~55 km, and there was no PMC correction in the Band 1 O_3. PMC interference in the Band 1 O_3 retrieval is removed using the PMC extinction measurements from Band 2, with an appropriate extrapolation in wavelength. This correction began in November 2009 when the band 2 detector came out of saturation. The 292 nm band is located in a region of strong O_3 absorption to provide enhanced sensitivity to O_3 in the mesosphere. This band provides O_3 measurements from roughly 105–50 km and is opaque at lower heights. The 330 nm band was selected to provide O_3 measurements

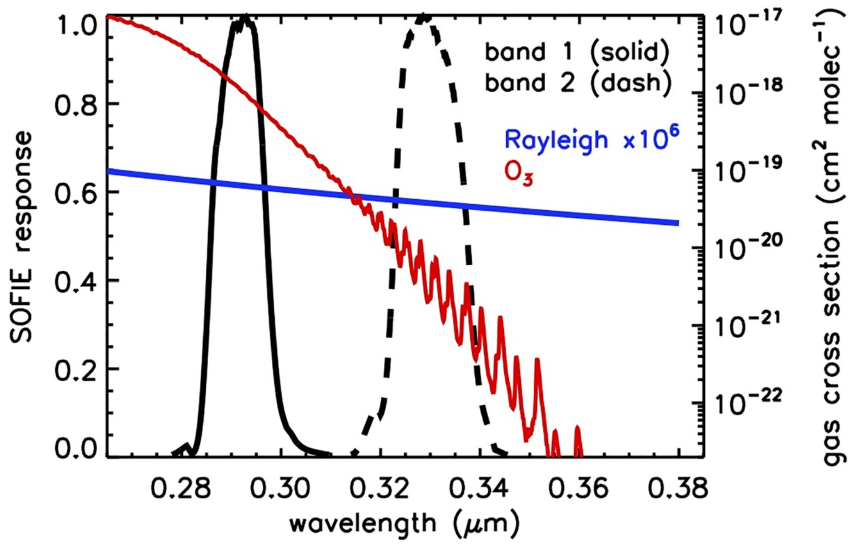

Figure 1. SOFIE spectral response and Rayleigh PMC interference in the O_3 bandpass spectral region. Using the channel 1 pair, O_3 is measured. Channel 1 is centered at 0.292 μm for strong (solid black curve) and 0.330 μm for weak (dashed black curve) O_3 bands.

from ∼60 km to the tropopause. Note that O_3 absorption at 330 nm is negligible above ∼60 km, and the Band 2 measurements there are used to characterize meteoric smoke (Hervig, Bardeen, et al., 2017, Hervig, Gordley, Russell, & Bailey, 2009; Herving et al., 2021) and PMCs during polar summer (Hervig et al., 2009a, 2009b). The transmission measurements from Bands 1 and 2 are used separately to retrieve O_3 vertical profiles. The two profiles are then merged to obtain a continuous O_3 product from ∼105 km altitude to the tropopause. The retrievals use O_3 simulations based on temperature-dependent O_3 cross-sections (Serdyuchenko et al., 2014). Refraction is described in full detail in the SOFIE forward model and thus is accounted for in the retrievals. Rayleigh scattering is the primary interference in the 292 and 330 nm bands. Rayleigh interference is calculated using optical cross-sections from Bodhaine et al. (1999) with SOFIE density measurements and removed during the retrieval process. The other interference in the O_3 bands is from stratospheric aerosols below ∼35 km (which is not corrected at this time) and from PMCs near 80–90 km during polar summer.

PMC (Hervig et al., 2009a, 2009b, 2013, 2016) contamination in the 292 nm O_3 measurements is successfully removed using the PMC extinction retrieved at 330 nm. For this purpose, the 330 nm PMC extinctions are extrapolated in wavelength to 292 nm, based on the modeled wavelength dependence described as the ratio of extinction at 292 nm to that for 330 nm. The extinction ratio varies with PMC particle size, but only by ±10% over the typical range (roughly 15–60 nm) of effective radius (r_e). For simplicity, the SOFIE approach assumes the long-term average r_e of 32 nm (Hervig et al., 2012) and accepts the resulting uncertainty (10%) in the O_3 mixing ratios retrieved in PMCs' presence. It is possible to instead use the retrieved r_e in the PMC corrections, which have uncertainties of up to ∼25%. Propagating these uncertainties into the O_3 retrieval, however, gives similar errors as assuming the long-term average r_e. Note that the Band 1 O_3 measurements are corrected for PMC interference only after November 2009, when the Band 2 measurements became operational.

2.3. SOFIE O_3 Uncertainty Analysis

SOFIE O_3 errors are due to uncertainties in either the observations or the forward model. Modeling errors include the description of interfering gases and aerosols and the representation of instrumental characteristics (e.g., relative spectral response or field of view). The V1.3 SOFIE O_3 forward model uses the optical cross-sections from Serdyuchenko et al. (2014), which are estimated to have 1% systematic uncertainties. The resulting uncertainties associated with the retrieved O_3 are determined by imposing each error mechanism in the V1.3 SOFIE retrieval algorithm. The approach applied known error sources to simulated observations and determined the resulting error from comparisons with the known O_3 profile. The results are summarized in Table 1, where the uncertainties in retrieved O_3 are summarized from 20 to 100 km altitude. The largest O_3 uncertainties are due to errors in

Table 1
O_3 Mixing Ratio Uncertainty (%) Due To Various Random (R) and Systematic (S) Error Mechanisms

	Altitude (km)								
Error source	20	30	40	50	60	70	80	90	100
Altitude registration (S)	5	3	3	3	2	2	2	2	2
Rayleigh interference (S)	2	1.5	1	2	0.5	1	1	0.5	1
Temperature bias (S)	1	1	1	1	1	1	2	3	5
O_3 Cross sections (S)	1	1	1	1	1	1	1	1	1
Field-of-view (S)	1	1	1.5	2	2	3	3	3	3
Forward model (S)	1	1	1	1	1	1	1	1	1
Signal noise (R)	0.5	0.1	0.1	0.15	0.1	0.1	0.15	0.2	1
Total (root sum squared)	5.8	3.9	3.9	4.5	3.4	4.1	4.5	4.9	6.5

Note. Retrievals are from Band 1 (292 nm) above ∼55 km and Band 2 (330 nm) at lower heights. Note that the uncertainties here do not address stratospheric aerosol or PMC interference.

the altitude registration, field of view calibration, and biases in temperature. Note that altitude registration errors are estimated to be 100 m (Marshall et al., 2010).

3. Correlative Data Sets

3.1. SCISAT ACE-FTS

ACE-FTS (Bernath, 2001; Bernath et al., 2005; Boone et al., 2005) is an instrument onboard the Canadian SciSat spacecraft and is a successor to the ATMOS (Atmospheric Trace Molecule Spectroscopy) experiment (Gunson et al., 1996). ACE uses solar occultation to measure minor species in Earth's atmosphere remotely. ACE was launched to low Earth orbit at 650 km and 74° inclination. ACE measures high-resolution (0.02 cm^{-1}) spectra of the atmosphere in the medium-long infrared range of 2.2–13 μm (Bernath et al., 2005). Using the occultation spectra, the vertical profiles of temperature, pressure, and VMRs of trace constituents are retrieved (Boone et al., 2005). The absence of adequately precise meteorological data for the entire ACE altitude range of observations necessitates the derivation of temperature and pressure directly from the ACE spectra as the first step of the retrieval. These profiles are used to calculate the synthetic spectra in the global fitting procedure to retrieve the VMR profiles of the target species in the second phase of the retrieval.

There were several accounts of the initial ACE O_3 validation comparisons for Version 1.0 (Fussen et al., 2005; Kerzenmacher et al., 2005; McHugh et al., 2005; Petelina et al., 2005; Walker et al., 2005). Froidevaux et al. (2006) used ACE version 2.1 O_3 in earlier validation studies for measurements from the Microwave Limb Sounder (MLS) on the Aura satellite. In these earlier O_3 retrievals, apparent discrepancies in the spectroscopic data near ∼5 and ∼10 μm were observed, due to which the vertical profiles near the stratospheric O_3 concentration peak had a low bias of ∼10% consistently compared to other satellite instruments' observations. An updated version 2.2 with improved spectroscopic measurements for O_3 was subsequently introduced and used in various validation studies (Cortesi et al., 2007; Dupuy et al., 2009; Froidevaux et al., 2008). In V2.2, O_3 VMRs are consistently larger than MLS, with O_3 profiles within 5% agreement in the lower stratosphere. However, the agreement deteriorates with altitude and reaches ∼25% at the upper stratosphere (Froidevaux et al., 2008). Cortesi et al. (2007) compared MIPAS V4.66 O_3 data with ACE V2.2 and reported that the relative difference was within ±10% between 10 and 42 km but deteriorated at higher altitudes, and Sheese et al. (2017) compared ACE-FTS V3.5 O_3 to correlative data from MIPAS and MLS. The difference in measurements between ACE, MLS, and MIPAS can be partly attributed to the difference in their measurement approach. ACE views a single latitude and makes 15 measurements in each hemisphere per day. MIPAS measures over a wide range of latitudes on a single day and during fixed local times. The Aura satellite, which has MLS aboard, is sun-synchronous at 705 km altitude with 98° inclination and provides a latitude coverage of 82° N to 82°S in each orbit. It has an ascending equator-crossing time of 1:45 p.m. and a 98.8-min period. In this study, we use ACE O_3 V4.1 data (Bernath et al., 2021). ACE makes ∼30 measurements per day, like SOFIE. However, it has a latitudinal coverage spread over the globe throughout the year due to the orbit inclination. Thus, there is limited coverage in the polar region.

The diurnal variation of O_3 along the line of sight is not accounted for in versions 3.6 and 4.1 of the ACE-FTS O_3 (Sheese et al., 2022).

3.2. Envisat MIPAS

The MIPAS instrument onboard the European ENVIronmental SATellite (ENVISAT) was operational from March 2002 until early April 2012. MIPAS was a middle infrared Fourier Transform spectrometer measuring high-resolution spectra of the atmospheric limb emission in five spectral bands (Fischer et al., 2008). ENVISAT was launched on a sun-synchronous polar orbit with 98.55° inclination and at ~800 km altitude.

MIPAS measured infrared spectra from 4.15 to 14.6 μm in the middle and upper atmosphere. This enabled the detection and spectral resolution of a large number of emission features of major and minor atmospheric constituents. The original spectral resolution of MIPAS was ~0.035 cm^{-1}. A reduced resolution of ~0.0625 cm^{-1} in a new operation mode was introduced in 2005. While the operational Level 2 MIPAS data are processed by ESA/DLR (European Space Agency/Deutsches Zentrum für Luft- und Raumfahrt); the University of Bologna, Oxford University, and the KIT-IMK/IAA (Karlsruhe Institute of Technology - Institute of Meteorology and Climate Research/Instituto de Astrofísica de Andalucía) are hosts to three other independent research Level-2 processors that rely on the same Level-1b ESA data but use different retrieval schemes. Overall, the four processors show similar performance, apply global fits, and use microwindows instead of the entire spectrum. Key differences in the processing schemes include the different regularization approaches (leading to a difference in the noise-resolution trade-off, with no clear average advantage to any specific data set), the choice of microwindows, the cloud detection threshold, and the approach to treating negative retrieved values.

We use the O_3 data processed by KIT-IMK/IAA. This data set has been used in several validation and investigative studies (Eckert et al., 2014; Glatthor et al., 2006; Laeng et al., 2014, 2018; López-Puertas et al., 2018; Steck et al., 2007; Stiller et al., 2012; von Clarmann et al., 2009). Laeng et al. (2014) validated MIPAS Version 5.0 (V5R_O3_224) O_3 data. López-Puertas et al. (2018) studied the O_3 in the middle atmosphere and determined the systematic and random errors in the 20–100 km range (at every 10 km). Version V5r_O3_m22 O_3 data in the stratosphere and mesosphere retrieved at 0.0625 cm^{-1} from 2005 to April 2012 in the microwindow of 14.8 and 10 μm spectral regions were used for observations made at three middle atmosphere modes (MA-Middle Atmosphere, NLC- Noctilucent and UA- Upper Atmosphere). During the daytime, MIPAS O_3 has an average vertical resolution of 3–4 km under 70 km. The average vertical resolution varies to 6–8 km at 70–80 km, 8–10 km at 80–90 km, and 5–7 km at the secondary O_3 maximum (90–100 km). López-Puertas et al. (2018) estimated the noise error for daytime to be typically smaller than 2% below 50 km, 2%–10% between 50 and 70 km, 10%–20% at 70–90 km, and ~30% above 95 km. They used SABER, ACE, MLS, and SMILES (Superconducting Submillimeter-Wave Limb-Emission Sounder (Baron et al., 2011; Imai et al., 2013; Kikuchi et al., 2010; Mitsuda et al., 2011; Takahashi et al., 2011)) to validate MIPAS O_3 and inferred that MIPAS agreed better than 5% with all instruments (except SABER) below 50 km. At the primary O_3 maximum, the difference was less than 5%. MIPAS measures 10%–20% less than SABER between 30 and 50 km and 5%–15% less in the stratospheric O_3 maximum. From 50 km to 65–70 km, MIPAS displays general agreement with all instruments (except SABER at 60–70 km and MLS at 65–70 km altitude range during some latitudes/seasons). The difference is less than 5%–10%, with MIPAS displaying higher O_3 values. MIPAS O_3 is smaller (5%–10%) than ACE-FTS from 45 to 55 km and had up to 20% less O_3 in the daytime than SABER from 50–60 km. The differences are higher above 60 km. The instruments are in good agreement at the secondary maximum except at certain latitudes/seasons. Overall, through all seasons, latitudes, and hemispheres, the MIPAS (V5r_O3_m22) O_3 during daytime has an accuracy of better than 5% at and below 50 km (with a positive bias of a few percent) and a positive bias of ~10% at 50–75 km (possibly due to spectroscopic errors). At 75–90 km, MIPAS shows a large relative positive difference with SMILES (10%–20%) and a negative difference (10%–50%) with SABER and ACE. MIPAS is accurate within 10%–20%. Above 90 km, MIPAS agrees with all instruments by 10%.

This study uses the most recent MIPAS retrieval, version 8.0, processed by KIT-IMK. O_3 VMR vertical distribution was retrieved for version 8 data products using different sets of microwindows above and below 70 km. The structure of the KIT processed MIPAS data is "spectra version_target species_baseline version" (e.g., V5R_O3_244 means that ESA spectra of version V5R (reduced spectral resolution) in IMK notation were used to retrieve target O_3 while a retrieval setup was used which is identified by the baseline number 244). This study uses baseline version 261 for all comparisons below 70 km and baseline versions 561 and 661 for altitudes above

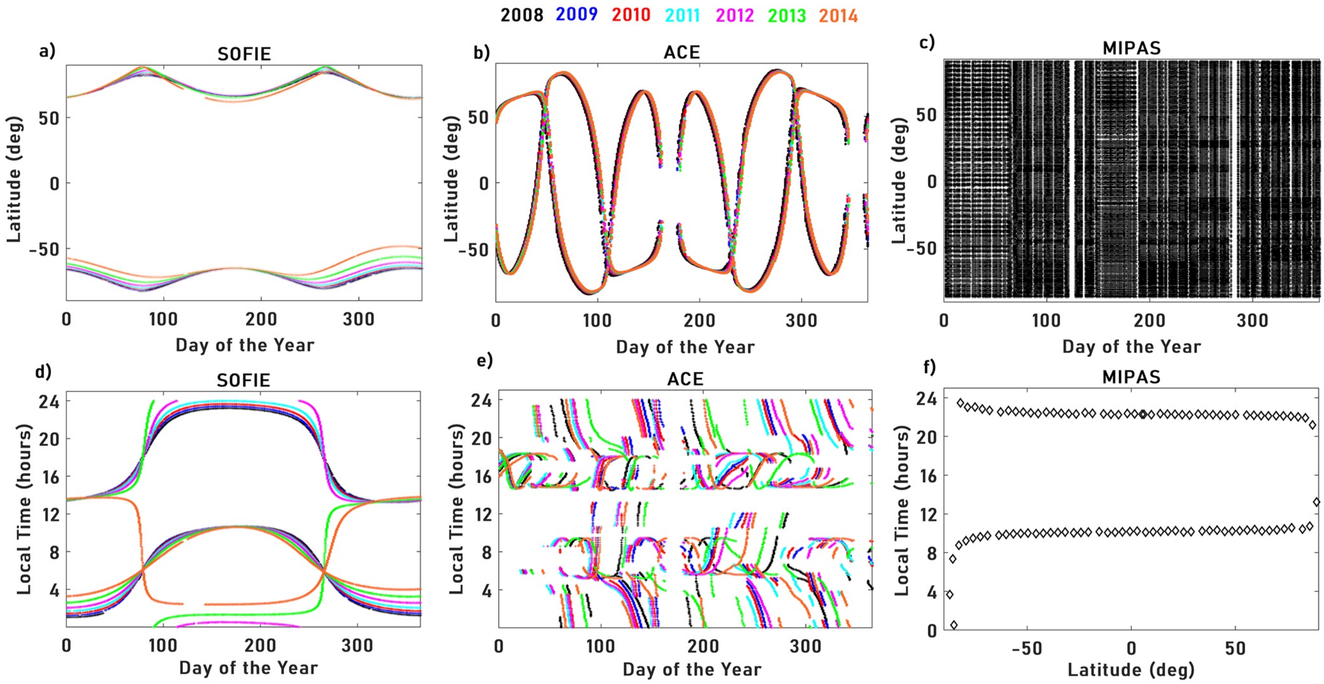

Figure 2. (a) SOFIE latitude coverages during 2008–2014 (b) ACE latitude coverages over years 2008–2014 (c) MIPAS latitude coverage for 2008, (d) SOFIE local time coverage during 2008–2014, (e) ACE local time coverage during 2008–2014, and (f) MIPAS local time variation with latitude.

70 km. While there are significant numbers of data points under baseline 261, the number of data points from versions 561 and 661 is relatively less. Since the Envisat mission ended in 2012, SOFIE measurements have been compared to coincident MIPAS O_3 profiles from 2008 to 2011. The systematic and random errors for MIPAS have been used as estimated by López-Puertas et al. (2018). An older version (Version 5r_O3_m22) of MIPAS was used to predict the error. Revised errors for version 8.0 O_3 were being worked on at the time of this writing.

4. Coincidence Analysis

Figures 2a–2c show the SOFIE, ACE, and MIPAS annual latitude coverages, respectively. SOFIE and ACE view a single latitude in each hemisphere on a given day, while MIPAS spans a wide latitude range on each day. Thus, the latitude coverage in Figure 2c is plotted for 2008 alone. 2009–2011 have a similar annual latitude distribution. Figures 2d and 2e show the SOFIE and ACE annual local time coverages, respectively. These coverages are from 2008 to 2014. Both SOFIE and ACE measure near local sunrise and sunset. Figure 2f shows the local time variation of MIPAS with latitude. For each orbit, Envisat's track repeated the same local times (~10:00 a.m./p.m.), with little daily or annual variation. Thus, Figure 2f indicates that there is little variation of local time with respect to latitude except at high polar latitudes.

4.1. Approach

The primary O_3 validation approach is to compare SOFIE with coincident measurements from ACE-FTS and MIPAS. The coincidence criteria are a latitude separation of ±5°, a longitude difference of ±20°, and a time separation of <2 hr (hereafter referred to as the coincidence box). During December, January, and February, there are very few coincidences between SOFIE and MIPAS. Thus, we use a time range of 3 hr during these months.

The monthly variation of coincidence numbers in both hemispheres is shown in Figure 3 (upper panel) for comparisons with ACE from 2008 to 2014 and in Figure 3 (lower panel) for comparisons with MIPAS. Although the number of coincidences per month is inconsistent (e.g., 0 in January and 114 in February in the NH), there are a large number of coincidences for each season. Figure 3 (lower panel) shows the number of coincident profiles between SOFIE and MIPAS from 2008 to 2011. MIPAS typically covers two local times. However, SOFIE has varying annual local time coverage. This leads to higher coincidence numbers between MIPAS and SOFIE,

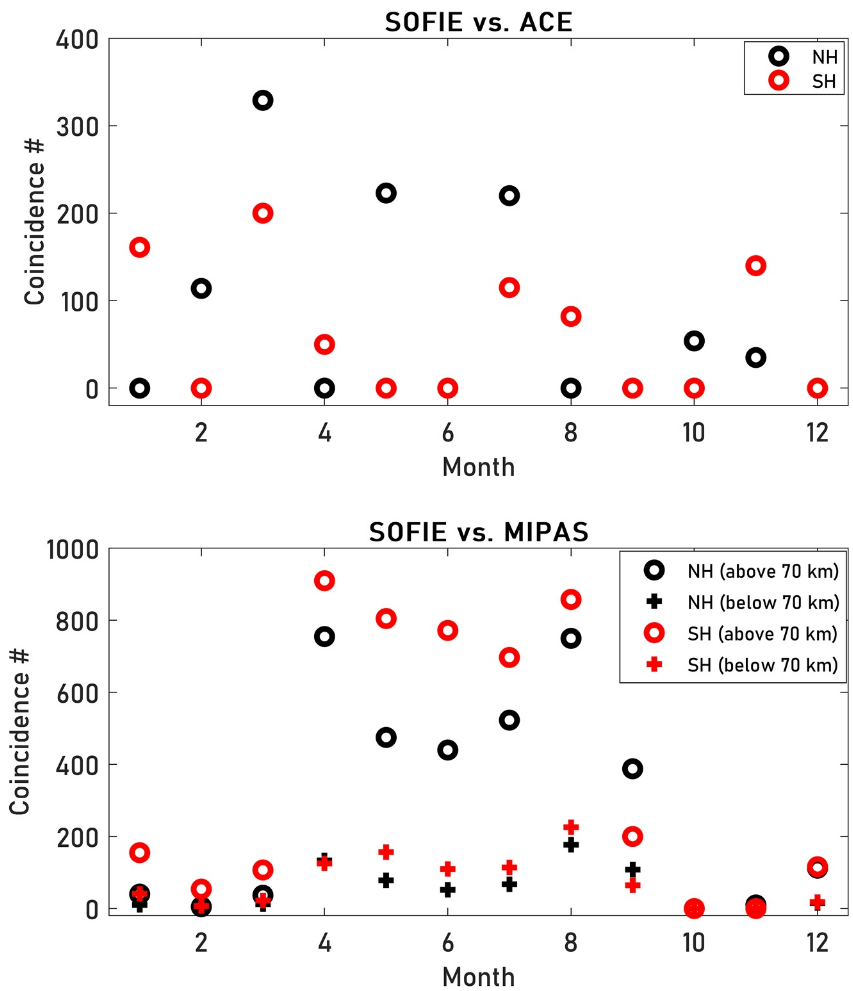

Figure 3. Monthly time series of the number of coincident profiles between (upper panel) SOFIE and ACE for 2008–2014 and (lower panel) SOFIE and MIPAS for 2008–2011. The coincidence box chosen is 20° in longitude × 5° in latitude × 2 hr in time (3 hr for DJF for MIPAS).

primarily during mid-year, from April to August. A different set of coincidences for MIPAS above and below 70 km have been calculated (Figure 3 (lower panel)) for reasons described in Section 3.2.

SOFIE has the highest vertical resolution compared to both ACE and MIPAS. SOFIE O_3 coincident profiles are linearly interpolated onto corresponding ACE and MIPAS grids. The SOFIE-ACE and SOFIE-MIPAS pairs' profiles are then linearly interpolated onto a common altitude grid of 2 km. A comparison between SOFIE and other correlative data sets is drawn by calculating the statistics at the common altitude grid.

The following statistics are used for the analysis of coincident O_3 VMR. The relative difference (δ_{rel}) is calculated using Equation 1.

$$\delta \mathrm{rel} = \frac{X_{\mathrm{SOFIE}} - X_{\mathrm{OTHER}}}{(X_{\mathrm{SOFIE}} + X_{\mathrm{OTHER}})/2} \tag{1}$$

The mean relative difference (Δ_{rel}) for N coincident points is calculated using Equation 2.

$$\Delta_{\mathrm{rel}} = \frac{1}{N} \sum_{i} \delta_i \tag{2}$$

The percent relative difference ($\Delta_{\mathrm{rel}(\%)}$) is calculated using Equation 3.

$$\Delta_{\mathrm{rel}}(\%) = \frac{1}{N} \sum_{i} \frac{(X(i)_{\mathrm{SOFIE}} - X(i)_{\mathrm{OTHER}}) \times 100}{(X(i)_{\mathrm{SOFIE}} + X(i)_{\mathrm{OTHER}})/2} \tag{3}$$

10.1029/2022EA002649

The 1σ standard deviation (SD) of the differences in percent (σ_{rel}) is calculated using Equation 4.

$$\sigma_{\mathrm{rel}} = \sqrt{\left(\frac{1}{N-1}\sum_{i}\left((\delta_i - \Delta_{\mathrm{rel}})^2\right)\right)} \tag{4}$$

The standard error of the mean difference (SEM) is calculated using Equation 5.

$$\mathrm{SEM} = \frac{\sigma_{\mathrm{rel}}}{N} \tag{5}$$

The random and systematic errors discussed in Section 2.3 factor into the statistics of combined error prediction. The SEM of the differences combined with the systematic errors of SOFIE and the correlative data set gives the total combined systematic error (Equation 6).

$$\mathrm{ErrorCombined}_{\mathrm{Systematic}} = \sqrt{\mathrm{SEM}^2 + \mathrm{Error}_{\mathrm{SOFIE}_{\mathrm{Systematic}}}{}^2 + \mathrm{Error}_{\mathrm{Correlated}_{\mathrm{Systematic}}}{}^2} \tag{6}$$

Random errors from SOFIE and the correlative data set are considered in calculating the total combined random error (Equation 7) (von Clarmann, 2006).

$$\mathrm{ErrorCombined}_{\mathrm{Random}} = \sqrt{\mathrm{Error}_{\mathrm{SOFIE}_{\mathrm{Random}}}{}^2 + \mathrm{Error}_{\mathrm{Correlated}_{\mathrm{Random}}}{}^2} \tag{7}$$

4.2. Statistics of the Coincidences

4.2.1. Winter

4.2.1.1. ACE

Figure 4 compares SOFIE with ACE during the winter for December, January, and February (DJF) in the NH and for June, July, and August (JJA) in the SH. Note that for Figures 4 through 7, panels a and d indicate the mean mixing ratio (VMR) values of all coincident profiles and the corresponding standard deviation of individual profiles from the mean in the NH and SH, respectively. Panels b and e indicate the mean number density profiles of the coincident profiles in the NH and SH, respectively, and the corresponding standard deviations are plotted using thin dashed lines with dots. Finally, panels c and f are used to show the statistical parameters calculated in Section 4.1 for the profiles shown in panels b and e, respectively. They show the mean difference, SD of the differences (%), and errors. For ACE, SOFIE's systematic and random errors are plotted, as these estimations are not currently reported for ACE. For MIPAS, the combined systematic and random errors are plotted. The analysis presented in this study has used coincident number density profiles to compare SOFIE and the other data sets. However, due to low number density values above ∼40 km, it is difficult to tell the mean number density profiles apart between SOFIE and the coincident instrument pair. Therefore, VMR profiles have been added to help distinguish the mean profiles at high altitudes.

In Figures 4a and 4d, the mean O_3 VMR profiles exhibit expected wintertime patterns in the stratosphere in both hemispheres. Patterns of gradual wintertime O_3 accumulations in the stratosphere tending toward a springtime maximum are evident. In the NH, all coincidences fall into February, which is late winter. Thus, all profiles are from the late winter period when the stratospheric O_3 build-up is at its peak. In the SH, the coincidences fall into July and August, with ∼17% higher coincidences in July than in August. Thus, the average of all profiles represents the average of mid and late-wintertime O_3. Hence, the accumulated wintertime stratospheric O_3 is better represented in the NH than in the SH.

For the NH, in Figure 4c, the mean difference values between SOFIE and ACE number density profiles are within 20% between 32 and 40 km and typically less than 10% between 40 and 70 km. At high altitudes, the mean difference values are less than 20% from 70 to 80 km and within 14% above this until 94 km. The mean differences are higher than 20% below ∼32 km and above ∼94 km, but typically under 50%. For the SH, in Figure 4e, the mean difference values are typically less than 30% between ∼34 and 90 km. At other altitudes from ∼20 to 100 km, the mean difference values are usually less than 40%. SOFIE results typically exhibit a low bias in the NH and the SH. Overall, there is better agreement between the instrument pair in the NH than in the SH.

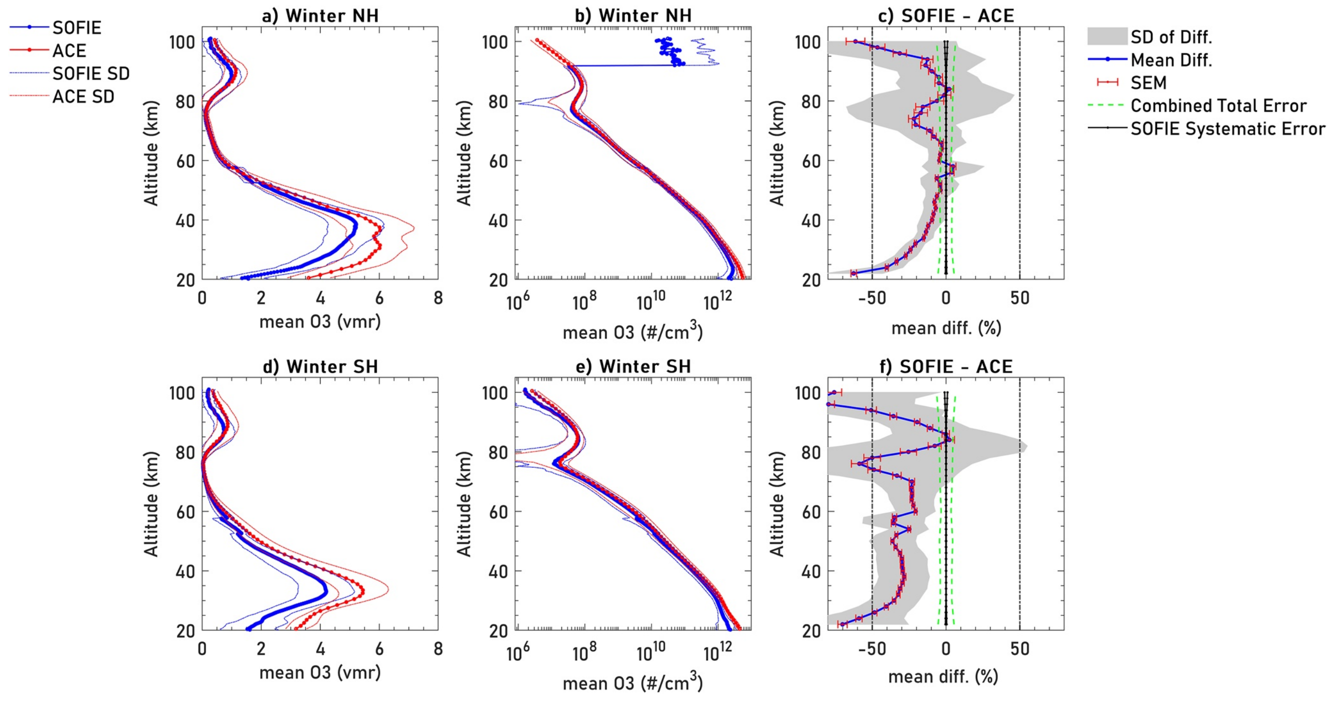

Figure 4. Statistics of coincident O_3 profiles from SOFIE and ACE for the winter. NH winter months DJF are plotted in panels (a)–(c), and SH winter months JJA are plotted in 4d, 4e, and 4f. Panels (a) and (c) indicate the mean values of all coincident profiles in terms of mixing ratio (VMR), and panels (b) and (e) indicate them in terms of number density (#/cm^3(log$_{10}$)) (blue for SOFIE and red for ACE). Panels (c) and (f) for SOFIE-ACE show the mean difference values between the number density profiles in percent (solid blue line with dots) with red SEM bars and the SD of the differences (gray shade). For SOFIE-ACE, the SOFIE systematic errors (green dashed lines), and SOFIE random errors (solid black line with dots) are plotted. The black dash lines with dots indicate the ±50% mean difference values.

4.2.1.2. MIPAS

Figures 5a and 5d show the coincident mean VMR profiles between SOFIE and MIPAS in the NH and SH, respectively, during the winter. Due to reasons explained in Section 3.2, the coincidences for the SOFIE-MIPAS pair are calculated separately above and below 70 km. Below 70 km, ~71% of the coincident profiles are in December and ~25% in January, with very few coincidences in February. Above 70 km, all coincidences are in December. Thus, the observations are biased toward early wintertime in the NH. The SOFIE-MIPAS pair in the NH capture the gradual wintertime enhancement in stratospheric O_3.

The number of coincident profiles in the SH has a relatively constant seasonal distribution. Below 70 km, ~33% of coincident profiles are in June, ~30% in July, and ~37% in August. Thus, the mean coincident profile is slightly biased toward late winter. Above 70 km, ~24% of coincident profiles are in December, ~34% in July, and ~50% in August. The wintertime stratospheric enhancement is less prominent in the SH than in NH. The limited representation of the wintertime stratospheric O_3 increase in the SH may be due to the averaging of the coincident profiles over 3 months not being equally weighted.

For both the NH and the SH, MIPAS measurements are typically higher than SOFIE at most altitudes. In the NH, for most altitudes from ~20 to 100 km, the mean difference values are less than 40% and typically tend to be higher above ~70 km. In the SH, the mean difference values are higher than in the NH and usually less than 50% below ~60 km. However, the mean difference values are higher than 50% above 70 km.

4.2.2. Non-Winter Months

4.2.2.1. ACE

Figure 6 compares SOFIE against ACE during all non-winter months, that is, from March through November in the NH and from September through May in the SH. Figures 6a and 6d show the O_3 vertical profiles in terms of VMR averaged over spring, summer, and fall months in the NH and SH, respectively. The corresponding number density profiles are plotted in Figures 6b and 6e, respectively. Due to the averaging of the O_3 profiles over all non-winter months, a trend in the stratospheric O_3 variability cannot be observed in the mean VMR profiles for

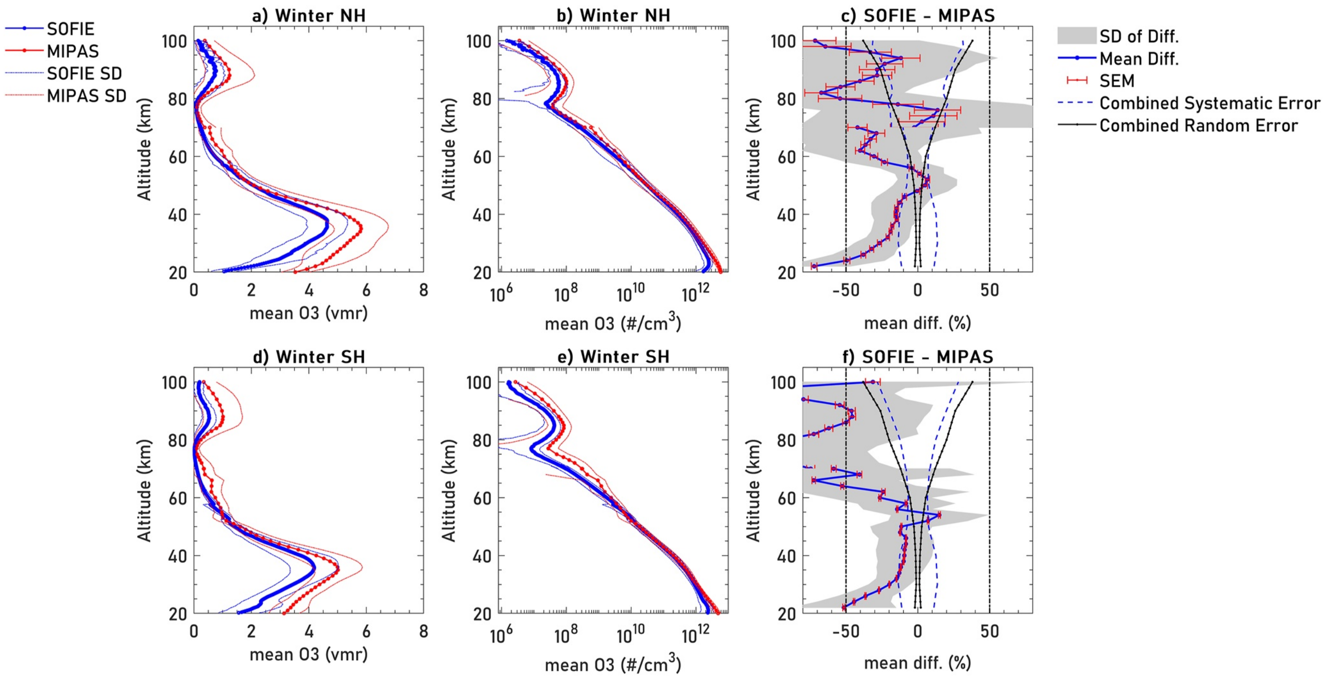

Figure 5. Statistics of coincident O_3 profiles from SOFIE and MIPAS for the winter. NH winter months DJF are plotted in panels (5a)–(5c), and SH winter months JJA are plotted in 5d, 5e, and 5f. Panels (a) and (c) indicate the mean values of all coincident profiles in terms of mixing ratio (VMR), and panels (b) and (e) indicate them in terms of number density (#/cm^3(log$_{10}$)) (blue for SOFIE and red for MIPAS). Panels (c) and (f) for SOFIE-MIPAS show the mean difference values in percent (solid blue line with dots) with red SEM bars and the SD of the differences (gray shade). The combined systematic (blue dashed line) and combined random errors (solid black line with dots) are plotted. The black dash lines with dots indicate the ±50% mean difference values.

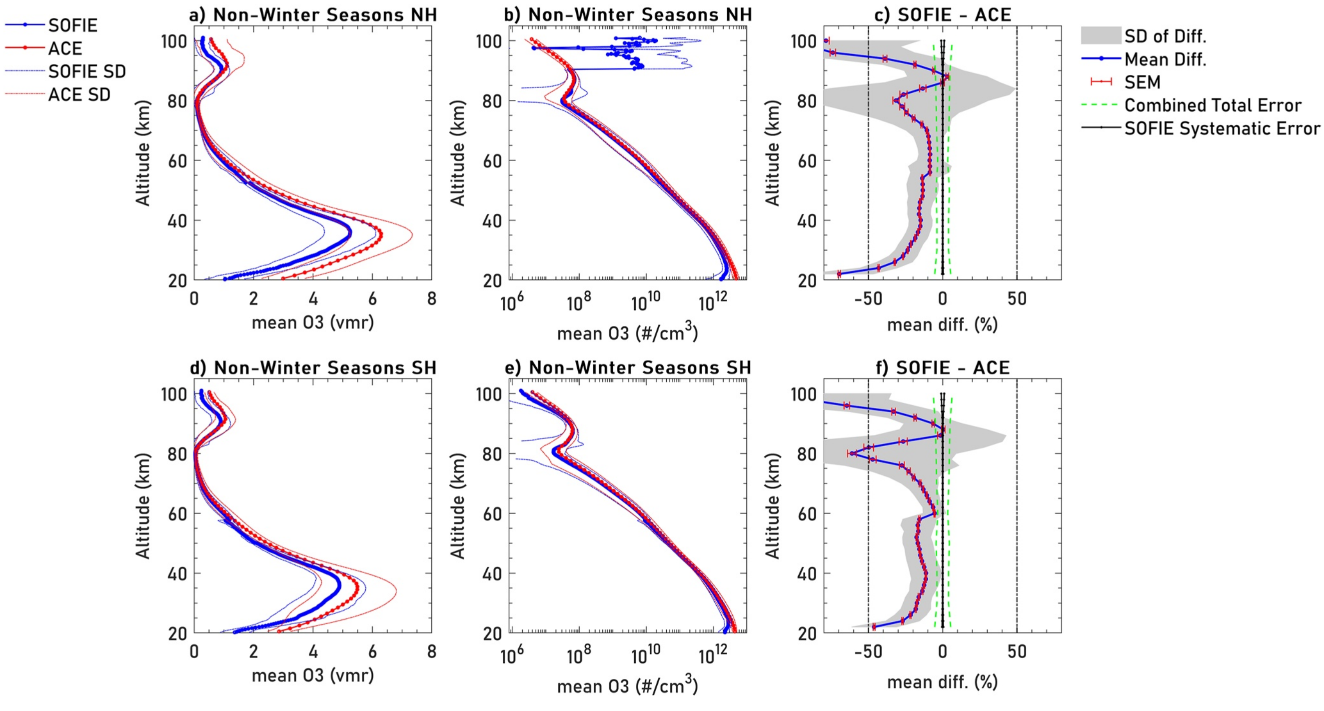

Figure 6. Same as Figure 4, but for all non-winter months, that is, March through November in the NH, and September through May in the SH.

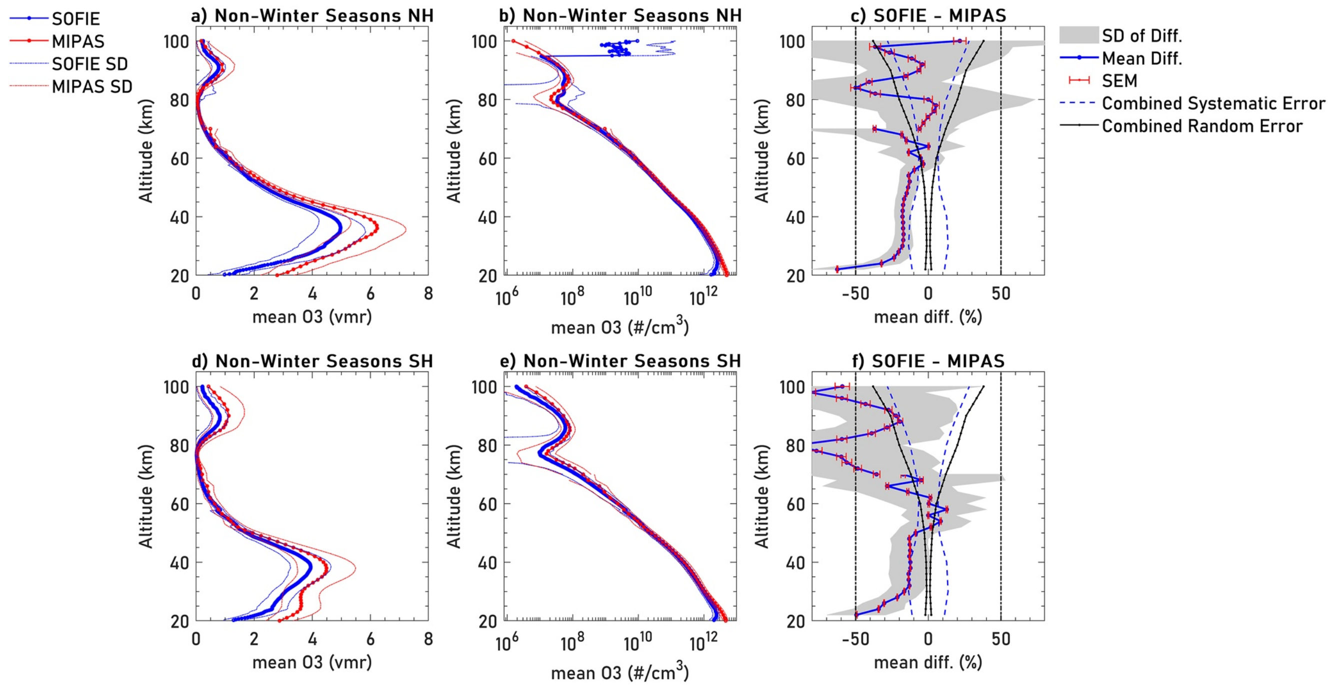

Figure 7. Same as Figure 5, but for all non-winter months, that is, March through November in the NH, and September through May in the SH.

either hemisphere. From Figure 6c, we gather that the mean differences between SOFIE and ACE are typically negatively biased in the NH, except near ~90 km. The values are less than—20% from ~30 to 90 km but are higher between ~74 and 84 km, as also seen during the winter. The values below ~30 km and above ~90 km are higher than—20% due to the large error values at these altitudes. In Figure 6f, the mean difference values in the SH are negatively biased except near ~90 km. Like in the NH, the differences are less than −20% between ~30 and 90 km but are higher between ~74 and 84 km. Below ~30 km, the values are higher than −20% but less than −50%. At altitudes above ~90 km, the mean difference values are higher than −20% and increase with altitude due to the high error values between 90 and 100 km. Overall, both hemispheres indicate similar bias values and agreement between SOFIE and ACE for the periods averaged over non-winter months, although, typically, the values at each altitude are slightly lower in the NH than the SH, suggesting better overall agreement in the NH.

4.2.2.2. MIPAS

Figure 7 shows the SOFIE-MIPAS comparisons during all non-winter months, that is, from March through November in the NH and from September through May in the SH. Figures 7a and 7d indicate the O_3 vertical profiles in terms of VMR averaged over spring, summer, and fall months in the NH and SH, respectively. The corresponding number density profiles are plotted in Figures 7b and 7e, respectively. Figure 7c suggests that in the NH, SOFIE is typically biased low at all altitudes except near ~80 km and at 100 km. The mean difference values are typically within −20% from ~30 to 90 km, except from ~74 to 84 km, where the values are higher but always less than −50%. Additionally, there is a brief digression at 70 km where the value is higher than −20%, and the data is discontinuous due to reasons explained in Section 3.2. The large mean differences near 20 km are consistent with the high SOFIE uncertainties (Table 1). In Figure 7f, the mean difference values in the SH indicate worse agreement between SOFIE and MIPAS in the SH than in the NH. The mean difference values between ~30 and 65 km are less than −20%, which is within the mutual uncertainties. As discussed earlier, the limited coincidences between SOFIE and MIPAS above 70 km and the high MIPAS noise errors above ~70 km (López-Puertas et al., 2018) explain the large systematic differences there. The presence of O_3 in very small amounts near 80 km explains the particularly large differences near that altitude. Additionally, the high diurnal variation in O_3 during sunrise contributes to the large differences between SOFIE and MIPAS above ~70 km.

The mean differences between SOFIE and other data sets over both hemispheres through the altitude range of ~20–100 km are summarized in Table 2. The values are shown at 10 km intervals in both hemispheres. The comparisons indicate qualitative and quantitative agreement between SOFIE and MIPAS, and ACE in terms of

Table 2

The Values Outside and Inside the Parenthesis Are the Mean Percent Differences Calculated From the Mean Number Density Profiles in the NH and SH, Respectively, Relative to SOFIE O_3 for ACE and MIPAS, at Different Altitudes[a]

	Altitude (km)								
Data set/Hemisphere	∼20	30	40	50	60	70	80	90	100
ACE winter (NH/SH)	−62.54	−24.06	−9.46	−4.47	−3.35	−11.06	−6.18	−9.65	−61.30
	(−70.10)	(−35.20)	(−29.33)	(−36.29)	(−20.59)	(−23.11)	(−25.47)	(−19.56)	(−75.70)
ACE Non-winter (NH/SH)	−69.57	−23.58	−14.81	−13.4	−8.78	−10.65	−31.40	−4.92	−78.52
	(−46.15)	(−17.33)	(−11.23)	(−16.75)	(−3.35)	(−15.26)	(−61.04)	(−6.46)	(>−80)
ACE total (NH/SH)	−66.05	−23.82	−12.13	−8.93	−6.06	−10.85	−18.79	−7.28	−69.91
	(−58.12)	(−26.26)	(−20.28)	(−26.52)	(−11.97)	(−19.18)	(−43.25)	(−13.01)	(>−77)
MIPAS winter (NH/SH)	−72.13	−26.67	−12.62	2.70	−30.46	−41.96	−67.13	−28.32	−71.44
	(−51.45)	(−19.79)	(−15.27)	(−11.44)	(−26.37)	(−74.48)	(>−80)	(−46.14)	(−31.34)
MIPAS non-winter	−62.57	−17.74	−17.77	−13.90	−5.50	−8.00	−0.09	−6.32	21.65
	(−49.40)	(−16.60)	(−12.62)	(−7.48)	(0.30)	(−17.32)	(>−80)	(−22.25)	(−59.14)
MIPAS total	−67.35	−22.20	−15.19	−8.30	−17.98	−24.98	−33.61	−17.32	−46.54
	(−50.42)	(−18.19)	(−13.94)	(−9.46)	(−13.03)	(−45.90)	(>−80)	(−34.19)	(−45.24)
Total	−66.70	−23.01	−13.66	−8.61	−12.02	−17.91	−26.20	−12.30	−58.22
	(−54.27)	(−22.22)	(−17.11)	(−17.99)	(−12.50)	(−32.54)	(>−61)	(−23.60)	(>−61)
Overall	−60.48	−22.61	−15.38	−13.30	−12.26	−25.22	>−43	−17.95	>−59

[a]The percent differences are calculated for altitudes at 10 km intervals, starting from ∼20 km, using the data plotted in Figures 4–7 of this paper. All cases combined for the same statistics are shown in the last row.

the mean seasonal climatology, where the mean difference values are less than 30% between ∼30 and 60 km when averaged over all hemispheres and seasons. SOFIE O_3 measurements typically indicate a low bias through all altitudes. Compared to ACE in the NH, the mean differences are typically less than 10% between 40 and 90 km. In the SH, the SOFIE-ACE differences are typically less than 30% from 20 to 90 km. Differences with MIPAS suggest that the difference values are less than −25% from 30 to 90 km, except at 80 km. In the SH, MIPAS shows higher differences but is within—25% from 30 to 90 km, except at 70 and 80 km.

The last row of Table 2 shows the average values of the NH and SH from SOFIE-ACE and SOFIE-MIPAS data pairs and represents the mean bias irrespective of the season, data set, and hemisphere. Comparisons of the differences between both data pairs indicate that there is a better overall agreement between SOFIE and ACE than between SOFIE and MIPAS. Although both data pairs show comparable overall agreement between ∼30 and 90 km, there are several altitudes in between where SOFIE agrees better with ACE than MIPAS. Due to the large random errors in MIPAS data above ∼70 km and the limited data points, the difference values above ∼70 km are less reliable. Differences higher than 30% near ∼80 km for both SOFIE-ACE and SOFIE-MIPAS comparisons are attributed to the small O_3 concentrations at these altitudes. High differences near ∼20 and ∼100 km occur due to the large error values at these altitudes. Additionally, Polar Stratospheric Cloud (PSC) interference near 20 km could be a possible reason behind the high mean difference values.

4.2.3. All Seasons

In Figure 8, we calculate the difference between the number density profiles for SOFIE and the other data sets for every season. SOFIE—ACE mean seasonal difference profiles in the NH and SH are plotted in Figures 8a and 8b, respectively. The mean seasonal profiles for SOFIE—MIPAS in the NH and SH are plotted in Figures 8c and 8d, respectively. For all panels, winter, spring, summer, and autumn are plotted in blue, green, red, and black, respectively.

In Figure 8a, all seasons indicate a similar trend in variability from 20 to 100 km. ACE measurements are typically higher than SOFIE through all altitudes and seasons. All seasons indicate mean difference values that are less than −20% between ∼30 and ∼90 km, except between ∼74 and 84 km, where the difference is higher. In the winter, the values are only slightly higher compared to other seasons. However, all seasons indicate a consistent pattern of high mean difference values between ∼74 and 84 km compared to the typical values observed from

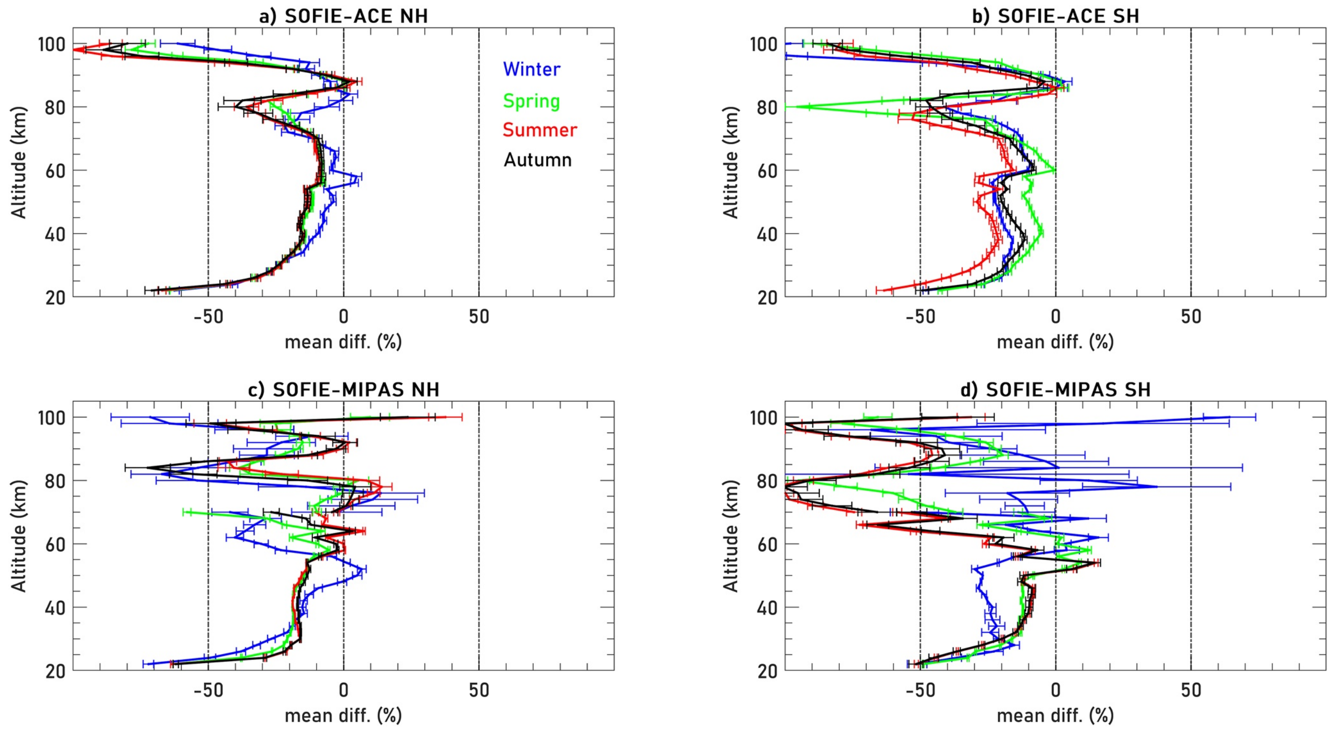

Figure 8. The mean difference profiles calculated for winter, spring, summer, and fall using the mean number density profiles are plotted for SOFIE-ACE in the (a) NH and (b) SH, and for SOFIE-MIPAS in the (c) NH and (d) SH. The black dash lines with dots indicate the −50%, 0%, and +50% mean difference values.

~30 to 90 km. Additionally, all seasons exhibit high mean difference values in the lower stratosphere or lower thermosphere. The mean difference values below ~25 km and above ~95 km are always higher than −50%. From Table 1, it is apparent that the highest total errors are reported at 20 and 100 km for SOFIE. Since ACE does not report its systematic and random errors, the uncertainty in measurements introduced at these altitudes by ACE cannot be quantified. However, larger than usual mean difference values near ~20 and ~100 km can be attributed in part to the high error values reported by SOFIE at these altitudes.

In Figure 8b, the SOFIE-ACE mean difference profiles over all seasons are typically less than −30% between ~30 and 90 km, except from ~74–84 km, where the values are higher. SOFIE results indicate low bias at almost all altitudes. Akin to the NH, the winter mean difference profile indicates lower values at most altitudes compared to other seasons between ~74 and 84 km. For the same reason as the NH, the mean difference values are higher than −50% for all seasons above ~95 km and close to −50% below ~25 km, except in the summer, where the mean difference is higher.

In Figure 8c, the SOFIE-MIPAS mean difference profiles in the NH for all seasons except winter indicate values less than −20% between ~35 and 75 km. Although the values at most altitudes that lie within this range are also less than −20% in the winter, the values are higher between ~55 and 70 km. The values above 70 km indicate a larger difference than −20% and are higher than −50% for a few altitudes in the winter and autumn. As discussed in Section 3.2, there are a limited number of coincidences between SOFIE and MIPAS above 70 km. Additionally, the noise error reported by López-Puertas et al. (2018), discussed in Section 3.2, indicates large values at altitudes above 70 km. The noise errors are typically 10%–20% between 70 and 90 km and 30% above 95 km. Overall, MIPAS indicated large differences (up to 50%) when compared to other data sets above 75 km, as described in Section 3.2.

In Figure 8d, the SOFIE-MIPAS mean difference values are less than −30% for all seasons from ~30 to 60 km. The values are higher below 30 km but always within −50%. As for the NH, the limited coincidences and the large noise errors above 70 km lead to large mean difference values.

5. Discussion

Figure 9 illustrates the solar occultation geometry in the plane containing the line of sight (LOS). In occultation experiments such as SOFIE, the optical depth and, thus, the abundance of the species along the LOS is related

10.1029/2022EA002649

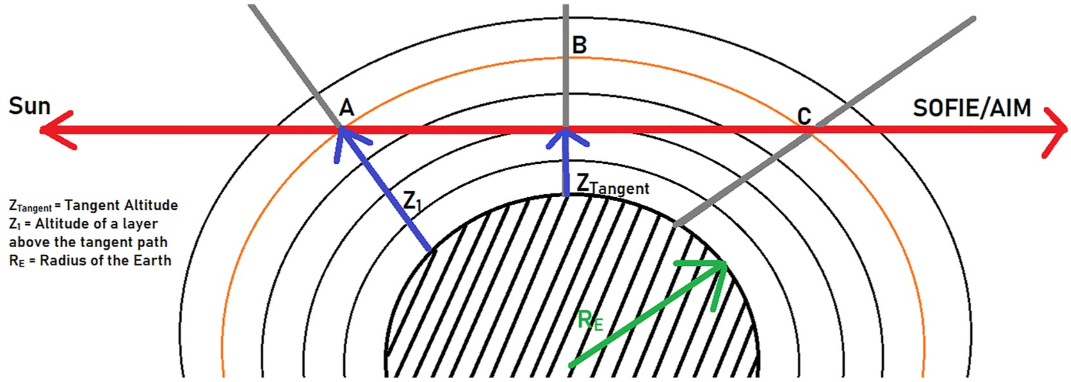

Figure 9. Schematic representation of the solar occultation measurement geometry. The red line indicates the LOS, $Z_{Tangent}$ is the tangent altitude, Z_1 is the altitude of a layer above the tangent altitude. Points A and C indicate the intersection of the layer at Z_1 with the LOS, where A is toward the sun and C is toward SOFIE/AIM. R_E is the radius of the Earth.

to the absorption of the solar radiance measured as a function of pressure or tangent height altitude. Typically, most of the absorption occurs around the tangent point due to the exponential decrease in atmospheric density with altitude and the slant path length established by the spherical geometry. Typical retrieval algorithms, as in the case of SOFIE, assume a horizontally homogeneous distribution of species in the atmosphere (Boone et al., 2005, 2013, 2020; Kroon et al., 2011). Because mesospheric O_3 has a short photochemical lifetime, its abundance will vary from day to night. While the entire SOFIE LOS exists in daylight, the spacecraft side of the LOS is closer to nighttime conditions, and thus, some gradient in O_3 is expected along the LOS.

Twilight variations have an impact on the interpretation of solar occultation measurements (Brohede et al., 2007; Boughner et al., 1980; Dube` et al., 2021; Gordley et al., 1996; Russel et al., 1988; Newchurch et al., 1996). Mesospheric O_3 has a short photochemical lifetime and, therefore, a sharp diurnal gradient. In such a situation, systematic errors may arise from the assumption of spherical symmetry. Such errors in O_3 abundance have been discussed for HALOE (version 19) by Natarajan et al. (2005). They used a diurnal photochemical model of mesospheric O_3 to derive correction factors to observations interpreted assuming spherical symmetry. Their analyses of model results suggest that at a tangent height of 61 km during January at the equator, neglecting twilight variations in mesospheric O_3 will underestimate the O_3 along the LOS by higher than 20% for sunrise and approximately 6% for sunset. Natarajan et al. (2023) investigated the bias introduced by neglecting the effects of twilight variations in the retrieval of O_3 in the mesosphere from SAGE III and implemented a correction scheme to provide an estimate of the bias in the standard retrieval. They used results from a diurnal photochemical model with different altitude inputs and developed a database of ratios of mesospheric O_3. This database was developed for various SZA values around 90° to mesospheric O_3 at a SZA of 90° for sunrise and sunset. Their results indicated that the twilight gradients have a higher impact during sunrise than sunset, and including the diurnal corrections during sunrise lowers the retrieved mesospheric O_3 by 30%. Additionally, they reported that neglecting the diurnal variation during June 2021 resulted in the overestimation of O_3 by 50% at 64 km at lower latitudes. Repeating the retrievals for January 2021 suggested larger differences near 70 km in the high latitude during winter due to a combination of low O_3 concentrations, large twilight correction factors, and large measurement uncertainties. The impact of diurnal variations on the O_3 data increases with altitude, necessitating larger correction at high altitudes.

Neither SOFIE nor ACE account for diurnal gradients in their retrievals. There may be systematic and random uncertainties, however, between the two as ACE utilizes infrared wavelengths and SOFIE UV; for a given altitude, the optical depths can be significantly different. Determining the magnitude of such biases is beyond the scope of this paper. We therefore conservatively estimate that agreement between SOFIE and ACE within 30% is reasonable. MIPAS makes observations at 10 a.m./p.m. local time. Diurnal variability between MIPAS local times and sunrise/sunset (as observed by SOFIE and ACE) indicates higher values during the local sunrise than sunset. The ratio between MIPAS O_3 measurements at 10 a.m. and 10 p.m. local time (at coincident locations and for the same day) indicates that the O_3 concentration is typically higher at 10 a.m. than at 10 p.m. from 20 to 100 km. O_3 values averaged from 20 to 100 km at 10 a.m. are ∼25% higher than the average at 10 p.m. Coincident O_3 measurements, when averaged from 65 to 80 km, indicate that for SOFIE and ACE, the relative difference is

−14.57% during sunrise and −1.56% during sunset. Coincident profiles, when averaged between 65 and 80 km for sunrise SOFIE and ∼midday MIPAS, indicate that the relative difference is −51.37%. SOFIE measurements compare better with ACE since these are both solar occultation instruments. Additionally, the high difference value relative to MIPAS is due to the limited MIPAS data points above ∼70 km. There are systematic differences between SOFIE and MIPAS above ∼70 km due to the limited coincidences and large uncertainties in the MIPAS data. These differences magnify at ∼80 km due to the small O_3 concentration near this altitude. However, with the given uncertainties, the mean difference values between SOFIE and MIPAS are typically less than 30% between 30 and 60 km during the winter and less than 20% for all other seasons averaged, where the values are less than ∼20% for most altitudes. Overall, SOFIE is biased low compared to ACE and MIPAS, shows good qualitative agreement, and reasonable quantitative agreement between ∼30 and 70 km. We, therefore, conclude that SOFIE O_3 is within the uncertainties of other data sets between ∼30 and 70 km and a valid data product for scientific use.

6. Summary and Conclusions

In this study, AIM SOFIE V1.3 O_3 data is compared to ACE-FTS V4.1/4.2 O_3 data, and Envisat MIPAS reprocessed V8.0 O_3 data set in the altitude range of 20–100 km. The statistics of coincident profiles, seasonal climatology, and the variation of the secondary O_3 maximum are investigated. The summary over all months (winter and non-winter) averaged, hemispheres and profile comparisons for the instrument pairs indicates that SOFIE O_3 agrees qualitatively at most altitudes and quantitatively (typically) between ∼30 and ∼70 km, and between ∼82 and 90 km (but not near 80 km due to the small O_3 values) with ACE and MIPAS regarding the mean state and the extent of variability. The mean difference values are less than 30% between ∼30 and 60 km. Over both hemispheres, all seasons, and data sets, SOFIE is biased low at all altitudes but more strongly in the lower stratosphere (∼20 km) and upper mesosphere (near 80 and 100 km). The large differences near ∼20 km are attributed to the high errors in this region and possibly due to PSC interference. Near ∼80 km, the high bias between SOFIE and both comparative data sets occurs due to the small O_3 concentration near this altitude. Large systematic and random errors reported by López-Puertas et al. (2018) for MIPAS, and the limited number of coincidences lead to high bias values near ∼100 km. Additionally, the large diurnal variability of O_3 during sunrise adds to the differences in both hemispheres.

The overall agreement between SOFIE and ACE is better in the NH than in the SH. The mean difference values averaged over all months are typically less than −20% between 40 and 90 km in the NH and less than −10% at several altitudes. In the SH, the overall agreement between SOFIE and ACE is less than −27% from 30 to 90 km, except near ∼80 km, where the values are higher. SOFIE and MIPAS difference values are typically less than −25% from 30 to 90 km in the NH when averaged over all months, with slightly higher values near ∼80 km. In the SH, SOFIE, and MIPAS show relatively less agreement at certain altitudes. The mean differences are typically less than −25% from 30 to ∼65 km, but higher values are observed above ∼70 km. The overall agreement between SOFIE and the correlative data sets is better in the NH than in the SH. The difference values averaged over all seasons and data sets indicate that the values are typically less than −25% from ∼30 to 90 km in the NH and less than −32% in the SH (except near ∼ 80 km). Mean differences averaged over both hemispheres suggest that SOFIE agrees best with the data sets from ∼30 to 90 km, with values typically less than −25% but higher values near ∼80 km due to the small O_3 concentration near this altitude.

There are two aspects of this analysis that need further evaluation. At the lower stratosphere (∼20 km), the O_3 values from SOFIE are much smaller than the correlative data sets, resulting in large mean differences in both hemispheres. A possible reason for SOFIE's low measurement could be the PSC signals that are not corrected. While the PSC contamination has a strong impact on the O_3 data, background sulfate aerosols contribute to scattering, are present in the atmosphere during all seasons, and have larger effects at lower altitudes. The sulfate aerosol interference isn't corrected by the current retrieval algorithm. An alternative explanation is that the destruction of O_3 by PSCs in the lower stratosphere is measured more accurately by SOFIE due to a higher number of near-pole measurements due to its continuous high latitude coverage. These measurements are within the latitude range of ±5° of the coincident profiles. Safieddine et al. (2020) and Tritscher et al. (2021) studied the destruction of O_3 by PSCs and the highly seasonal nature of the losses. Further analysis of SOFIE O_3 with comparisons to ozonesonde data will be useful in evaluating the extent of the O_3 loss due to PSCs. Typically, SOFIE shows high bias values compared to other data sets between ∼20 and 30 km. Although the current V1.3 reports O_3 data at these altitudes, future SOFIE versions will use more refined reporting altitudes. A second irregularity is a sudden increase in the mean difference between SOFIE and the correlative data sets and the low values of SOFIE O_3 near ~80 km. SOFIE O_3 data was corrected for polar mesospheric cloud (PMC) interference after 2009. The data prior to 2009 consists of PMC interference during the polar summer (mid-May to late August in the NH and late November to late February in the SH). Thus, 2008 data from SOFIE O_3 during these periods possibly impacted the O_3, leading to higher mean difference values at ~80 km. However, the overall data quality is not affected by these biases.

SOFIE O_3 observations agree with ACE and MIPAS overall, and the mean differences are typically less than 30% between 30 and 60 km. The seasonal differences indicate a similar trend over all seasons. Our results demonstrate the utility and robustness of the SOFIE O_3 data product.

Data Availability Statement

Level 2 SOFIE version 1.3 data are used in this study for temperature and ozone (SOFIE, 2007). ACE version 4.1 data are used in this study for temperature and ozone (ACE, 2004 (registration required)). MIPAS Version 8.0 data processed by the Karlsruhe Institute of Technology for ozone are used in this study (Karlsruhe Institute of Technology, 2002 (registration required)). Figures were made using Matlab version R2022a, available under the Matlab license at https://www.mathworks.com/pricing-licensing.html.

Acknowledgments

The AIM mission and SOFIE observations are funded by NASA's Small Explorers Program. This work was funded by NASA Grant NNX17AD25G. We thank the SOFIE and AIM operation teams for their help and excellent support with this work. We thank the ACE team for their data. The Canadian Space Agency funds ACE. We thank the Karlsruhe Institute of Technology for providing processed MIPAS data.

References

ACE Science Team. (2004). ACE V4.1/4.2 temperature (T), and ozone (O_3) products [Dataset]. ACE Science Team. Retrieved from https://databace.scisat.ca/level2/ace_v4.1_v4.2/

Adams, C., Bourassa, A. E., Sofieva, V., Froidevaux, L., McLinden, C. A., Hubert, D., et al. (2014). Assessment of Odin-OSIRIS ozone measurements from 2001 to the present using MLS, GOMOS, and ozone sondes. *Atmospheric Measurement Techniques Discussions*, *6*(2), 3819–3857. https://doi.org/10.5194/amt-7-49-2014

Adams, C., Strong, K., Batchelor, R. L., Bernath, P. F., Brohede, S., Boone, C., et al. (2012). Validation of ACE and OSIRIS ozone and NO_2 measurements using ground-based instruments at 80° N. *Atmospheric Measurement Techniques Discussions*, *5*(1), 517–588. https://doi.org/10.5194/amt-5-927-2012

Baron, P., Urban, J., Sagawa, H., Möller, J., Murtagh, D. P., Mendrok, J., et al. (2011). The level 2 research product algorithms for the superconducting submillimeter-wave limb-emission sounder (SMILES). *Atmospheric Measurement Techniques*, *4*(10), 2105–2124. https://doi.org/10.5194/amt-4-2105-2011

Bernath, P. (2001). Atmospheric chemistry experiment (ACE): An overview. Spectroscopy from Space (pp. 147–160).

Bernath, P. F., Crouse, J., Hughes, R. C., & Boone, C. D. (2021). The atmospheric chemistry experiment Fourier transform spectrometer (ACE-FTS) version 4.1 retrievals: Trends and seasonal distributions. *Journal of Quantitative Spectroscopy and Radiative Transfer*, *259*, 107409. https://doi.org/10.1016/j.jqsrt.2020.107409

Bernath, P. F., McElroy, C. T., Abrams, M. C., Boone, C. D., Butler, M., Camy-Peyret, C., et al. (2005). Atmospheric chemistry experiment (ACE): Mission overview. *Geophysical Research Letters*, *32*(15), L15S01. https://doi.org/10.1029/2005GL022386

Bodeker, G. E., Shiona, H., & Eskes, H. (2005). Indicators of Antarctic ozone depletion. *Atmospheric Chemistry and Physics*, *5*(10), 2603–2615. https://doi.org/10.5194/acp-5-2603-2005

Bodhaine, B. A., Wood, N. B., Dutton, E. G., & Slusser, J. R. (1999). On Rayleigh optical depth calculations. *Journal of Atmospheric and Oceanic Technology*, *16*(11), 1854–1861. https://doi.org/10.1175/1520-0426(1999)016%3C1854:ORODC%3E2.0.CO;2

Bognar, K., Tegtmeier, S., Bourassa, A., Roth, C., Warnock, T., Zawada, D., & Degenstein, D. (2022). Stratospheric ozone trends for 1984–2021 in the SAGE II–OSIRIS–SAGE III/ISS composite dataset. *Atmospheric Chemistry and Physics*, *22*(14), 9553–9569. https://doi.org/10.5194/acp-22-9553-2022

Boone, C. D., Bernath, P. F., Cok, D., Jones, S. C., & Steffen, J. (2020). Version 4 retrievals for the atmospheric chemistry experiment Fourier transform spectrometer (ACE-FTS) and imagers. *Journal of Quantitative Spectroscopy and Radiative Transfer*, *247*, 106939. https://doi.org/10.1016/j.jqsrt.2020.106939

Boone, C. D., Nassar, R., Walker, K. A., Rochon, Y., McLeod, S. D., Rinsland, C. P., & Bernath, P. F. (2005). Retrievals for the atmospheric chemistry experiment Fourier-transform spectrometer. *Applied Optics*, *44*(33), 7218–7231. https://doi.org/10.1364/ao.44.007218

Boone, C. D., Walker, K. A., & Bernath, P. F. (2013). Version 3 retrievals for the atmospheric chemistry experiment Fourier transform spectrometer (ACE-FTS). *The atmospheric chemistry experiment ACE at*, *10*, 103–127.

Boughner, R., Larsen, J. C., & Natarajan, M. (1980). The influence of NO and CℓO variations at twilight on the interpretation of solar occultation measurements. *Geophysical Research Letters*, *7*(4), 231–234. https://doi.org/10.1029/GL007i004p00231

Bourassa, A. E., Roth, C. Z., Zawada, D. J., Rieger, L. A., McLinden, C. A., & Degenstein, D. A. (2018). Drift-corrected odin-OSIRIS ozone product: Algorithm and updated stratospheric ozone trends. *Atmospheric Measurement Techniques*, *11*(1), 489–498. https://doi.org/10.5194/amt-11-489-2018

Bovensmann, H., Burrows, J. P., Buchwitz, M., Frerick, J., Noel, S., Rozanov, V. V., et al. (1999). SCIAMACHY: Mission objectives and measurement modes. *Journal of the Atmospheric Sciences*, *56*(2), 127–150. https://doi.org/10.1175/1520-0469(1999)056%3C0127:SMOAMM%3E2.0.CO;2

Brohede, S. M., Haley, C. S., McLinden, C. A., Sioris, C. E., Murtagh, D. P., Petelina, S. V., et al. (2007). Validation of Odin/OSIRIS stratospheric NO2 profiles. *Journal of Geophysical Research*, *112*(D7), D07310. https://doi.org/10.1029/2006JD007586

Chipperfield, M. P., Bekki, S., Dhomse, S., Harris, N. R. P., Hassler, B., Hossaini, R., et al. (2017). Detecting recovery of the stratospheric ozone layer. *Nature*, *549*, 211–218. https://doi.org/10.1038/nature23681

Chipperfield, M. P., Feng, W., & Rex, M. (2005). Arctic ozone loss and climate sensitivity: Updated three-dimensional model study. *Geophysical Research Letters*, *32*(11), L11813. https://doi.org/10.1029/2005GL022674

Chubachi, S. (1984). Preliminary result of ozone observations at Syowa from February 1982 to January 1983. *Memoirs of National Institute of Polar Research, Special Issue*, *34*, 13–19.

Cisewski, M., Zawodny, J., Gasbarre, J., Eckman, R., Topiwala, N., Rodriguez-Alvarez, O., et al. (2014). The stratospheric aerosol and gas experiment (SAGE III) on the International Space Station (ISS) Mission. In *Sensors, systems, and next-generation satellites XVIII* (Vol. 9241, pp. 59–65). SPIE. https://doi.org/10.1117/12.2073131

Clarmann, T. V., De Clercq, C., Ridolfi, M., Hoepfner, M., & Lambert, J. C. (2009). The horizontal resolution of MIPAS. *Atmospheric Measurement Techniques*, *2*(1), 47–54. https://doi.org/10.5445/IR/1000041684

Cortesi, U., Lambert, J. C., De Clercq, C., Bianchini, G., Blumenstock, T., Bracher, A., et al. (2007). Geophysical validation of MIPAS-ENVISAT operational ozone data. *Atmospheric Chemistry and Physics*, *7*(18), 4807–4867. https://doi.org/10.5194/acp-7-4807-2007

Cracknell, A. P., & Varotsos, C. (2012). *Remote sensing and atmospheric ozone: Human activities versus natural variability*. Springer Science & Business Media.

Cunnold, D. M., Chu, W. P., Barnes, R. A., McCormick, M. P., & Veiga, R. E. (1989). Validation of SAGE II ozone measurements. *Journal of Geophysical Research*, *94*(D6), 8447–8460. https://doi.org/10.1029/JD094iD06p08447

De Laat, A. T. J., & Van Weele, M. (2011). The 2010 Antarctic ozone hole: Observed reduction in ozone destruction by minor sudden stratospheric warmings. *Scientific Reports*, *1*(1), 38. https://doi.org/10.1038/srep00038

Dubé, K., Bourassa, A., Zawada, D., Degenstein, D., Damadeo, R., Flittner, D., & Randel, W. (2021). Accounting for the photochemical variation in stratospheric NO_2 in the SAGE III/ISS solar occultation retrieval. *Atmospheric Measurement Techniques*, *14*(1), 557–566. https://doi.org/10.5194/amt-14-557-2021

Dupuy, E., Walker, K. A., Kar, J., Boone, C. D., McElroy, C. T., Bernath, P. F., et al. (2009). Validation of ozone measurements from the atmospheric chemistry experiment (ACE). *Atmospheric Chemistry and Physics*, *9*(2), 287–343. https://doi.org/10.5194/acp-9-287-2009

Eckert, E., von Clarmann, T., Kiefer, M., Stiller, G. P., Lossow, S., Glatthor, N., et al. (2014). Drift-corrected trends and periodic variations in MIPAS IMK/IAA ozone measurements. *Atmospheric Chemistry and Physics*, *14*(5), 2571–2589. https://doi.org/10.5194/acp-14-2571-2014

Farman, J. C., Gardiner, B. G., & Shanklin, J. D. (1985). Large losses of total ozone in Antarctica reveal seasonal ClOx/NOx interaction. *Nature*, *315*, 207–210. https://doi.org/10.1038/315207a0

Fischer, H., Birk, M., Blom, C., Carli, B., Carlotti, M., Von Clarmann, T., et al. (2008). MIPAS: An instrument for atmospheric and climate research. *Atmospheric Chemistry and Physics*, *8*(8), 2151–2188. https://doi.org/10.5194/acp-8-2151-2008

Flynn, L., Long, C., Wu, X., Evans, R., Beck, C. T., Petropavlovskikh, I., et al. (2014). Performance of the ozone mapping and profiler suite (OMPS) products. *Journal of Geophysical Research: Atmospheres*, *119*(10), 6181–6195. https://doi.org/10.1002/2013JD020467

Flynn, L. E., Seftor, C. J., Larsen, J. C., & Xu, P. (2006). The ozone mapping and profiler suite. In *Earth science satellite remote sensing: Vol. 1: Science and instruments* (pp. 279–296). Springer Berlin Heidelberg.

Froidevaux, L., Jiang, Y. B., Lambert, A., Livesey, N. J., Read, W. G., Waters, J. W., et al. (2008). Validation of Aura microwave limb sounder HCl measurements. *Journal of Geophysical Research*, *113*(D15), D15S25. https://doi.org/10.1029/2007jd009025

Froidevaux, L., Livesey, N. J., Read, W. G., Jiang, Y. B., Jimenez, C., Filipiak, M. J., et al. (2006). Early validation analyses of atmospheric profiles from EOS MLS on the Aura satellite. *IEEE Transactions on Geoscience and Remote Sensing*, *44*(5), 1106–1121. https://doi.org/10.1109/TGRS.2006.864366

Fussen, D., Vanhellemont, F., Dodion, J., Bingen, C., Walker, K. A., Boone, C. D., et al. (2005). Initial intercomparison of ozone and nitrogen dioxide number density profiles retrieved by the ACE-FTS and GOMOS occultation experiments. *Geophysical Research Letters*, *32*(16), L16S02. https://doi.org/10.1029/2005GL022468

Glatthor, N., Von Clarmann, T., Fischer, H., Funke, B., Gil-López, S., Grabowski, U., et al. (2006). Retrieval of stratospheric ozone profiles from MIPAS/ENVISAT limb emission spectra: A sensitivity study. *Atmospheric Chemistry and Physics*, *6*(10), 2767–2781. https://doi.org/10.5194/acp-6-2767-2006

Gordley, L., Burton, J., Marshall, B. T., McHugh, M., Deaver, L., Nelsen, J., et al. (2009b). High precision refraction measurements by solar imaging during occultation: Results from SOFIE. *Applied Optics*, *48*(25), 4814–4825. https://doi.org/10.1364/AO.48.004814

Gordley, L. L., Hervig, M. E., Fish, C., Russell, J. M., III, Bailey, S., Cook, J., et al. (2009a). The solar occultation for ice experiment. *Journal of Atmospheric and Solar-Terrestrial Physics*, *71*(3–4), 300–315. https://doi.org/10.1016/j.jastp.2008.07.012

Gordley, L. L., Marshall, B. T., & Chu, D. A. (1994). LINEPAK: Algorithms for modeling spectral transmittance and radiance. *Journal of Quantitative Spectroscopy and Radiative Transfer*, *52*(5), 563–580. https://doi.org/10.1016/0022-4073(94)90025-6

Gordley, L. L., Russell, J. M., III, Mickley, L. J., Frederick, J. E., Park, J. H., Stone, K. A., et al. (1996). Validation of nitric oxide and nitrogen dioxide measurements made by the Halogen Occultation Experiment for UARS platform. *Journal of Geophysical Research*, *101*(D6), 10241–10266. https://doi.org/10.1029/95JD02143

Gunson, M. R., Abbas, M. M., Abrams, M. C., Allen, M., Brown, L. R., Brown, T. L., et al. (1996). The atmospheric trace molecule spectroscopy (ATMOS) experiment: Deployment on the ATLAS space shuttle missions. *Geophysical Research Letters*, *23*(17), 2333–2336. https://doi.org/10.1029/96GL01569

Hervig, M. E., Bardeen, C. G., Siskind, D. E., Mills, M. J., & Stockwell, R. (2017). Meteoric smoke and H_2SO_4 aerosols in the upper stratosphere and mesosphere. *Geophysical Research Letters*, *44*(2), 1150–1157. https://doi.org/10.1002/2016GL072049

Hervig, M. E., Berger, U., & Siskind, D. E. (2016). Decadal variability in PMCs and implications for changing temperature and water vapor in the upper mesosphere. *Journal of Geophysical Research: Atmospheres*, *121*(5), 2383–2392. https://doi.org/10.1002/2015JD024439

Hervig, M. E., Brooke, J. S., Feng, W., Bardeen, C. G., & Plane, J. M. (2017). Constraints on meteoric smoke composition and meteoric influx using SOFIE observations with models. *Journal of Geophysical Research: Atmospheres*, *122*(24), 13–495. https://doi.org/10.1002/2017JD027657

Hervig, M. E., Deaver, L. E., Bardeen, C. G., Russell, J. M., III, Bailey, S. M., & Gordley, L. L. (2012). The content and composition of meteoric smoke in mesospheric ice particles from SOFIE observations. *Journal of Atmospheric and Solar-Terrestrial Physics*, *84*, 1–6. https://doi.org/10.1016/j.jastp.2012.04.005

Hervig, M. E., Gordley, L. L., Russell, J. M., III, & Bailey, S. M. (2009a). SOFIE PMC observations during the northern summer of 2007. *Journal of Atmospheric and Solar-Terrestrial Physics*, *71*(3–4), 331–339. https://doi.org/10.1016/j.jastp.2008.08.010

Hervig, M. E., Gordley, L. L., Stevens, M. H., Russell, J. M., III, Bailey, S. M., & Baumgarten, G. (2009b). Interpretation of SOFIE PMC measurements: Cloud identification and derivation of mass density, particle shape, and particle size. *Journal of Atmospheric and Solar-Terrestrial Physics*, *71*(3–4), 316–330. https://doi.org/10.1016/j.jastp.2008.07.009

Hervig, M. E., Plane, J. M., Siskind, D. E., Feng, W., Bardeen, C. G., & Bailey, S. M. (2021). New global meteoric smoke observations from SOFIE: Insight regarding chemical composition, meteoric influx, and hemispheric asymmetry. *Journal of Geophysical Research: Atmospheres*, *126*(13), e2021JD035007. https://doi.org/10.1029/2021JD035007

Hervig, M. E., Siskind, D. E., Stevens, M. H., & Deaver, L. E. (2013). Inter-hemispheric comparison of PMCs and their environment from SOFIE observations. *Journal of Atmospheric and Solar-Terrestrial Physics*, *104*, 285–298. https://doi.org/10.1016/j.jastp.2012.10.013

Imai, K., Manago, N., Mitsuda, C., Naito, Y., Nishimoto, E., Sakazaki, T., et al. (2013). Validation of ozone data from the superconducting submillimeter-wave limb-emission sounder (SMILES). *Journal of Geophysical Research: Atmospheres*, *118*(11), 5750–5769. https://doi.org/10.1002/jgrd.50434

Jiang, Y. B., Froidevaux, L., Lambert, A., Livesey, N. J., Read, W. G., Waters, J. W., et al. (2007). Validation of aura microwave limb sounder ozone by ozonesonde and lidar measurements. *Journal of Geophysical Research*, *112*(D24), D24S34. https://doi.org/10.1029/2007JD008776

Karlsruhe Institute of Technology generated MIPAS data. (2002). The MIPAS V 8 temperature (Temperature), and ozone (O_3) products [Dataset]. Karlsruhe Institute of Technology. Retrieved from https://www.imk-asf.kit.edu/english/308.php

Kerzenmacher, T. E., Walker, K. A., Strong, K., Berman, R., Bernath, P. F., Boone, C. D., et al. (2005). Measurements of O_3, NO_2 and temperature during the 2004 Canadian Arctic ACE validation campaign. *Geophysical Research Letters*, *32*(16), L16S07. https://doi.org/10.1029/2005GL023032

Kikuchi, K. I., Nishibori, T., Ochiai, S., Ozeki, H., Irimajiri, Y., Kasai, Y., et al. (2010). Overview and early results of the superconducting submillimeter-wave limb-emission sounder (SMILES). *Journal of Geophysical Research*, *115*(D23), D23306. https://doi.org/10.1029/2010jd014379

Kramarova, N. A., Nash, E. R., Newman, P. A., Bhartia, P. K., McPeters, R. D., Rault, D. F., et al. (2014). Measuring the Antarctic ozone hole with the new ozone mapping and profiler suite (OMPS). *Atmospheric Chemistry and Physics*, *14*(5), 2353–2361. https://doi.org/10.5194/acp-14-2353-2014

Kroon, M., De Haan, J. F., Veefkind, J. P., Froidevaux, L., Wang, R., Kivi, R., & Hakkarainen, J. J. (2011). Validation of operational ozone profiles from the ozone monitoring instrument. *Journal of Geophysical Research*, *116*(D18), D18305. https://doi.org/10.1029/2010JD015100

Kuttippurath, J., Feng, W., Müller, R., Kumar, P., Raj, S., Gopikrishnan, G. P., & Roy, R. (2021). Exceptional loss in ozone in the Arctic winter/spring of 2019/2020. *Atmospheric Chemistry and Physics*, *21*(18), 14019–14037. https://doi.org/10.5194/acp-21-14019-2021

Kuttippurath, J., Godin-Beekmann, S., Lefèvre, F., Santee, M. L., Froidevaux, L., & Hauchecorne, A. (2015). Variability in Antarctic ozone loss in the last decade (2004–2013): High-resolution simulations compared to aura MLS observations. *Atmospheric Chemistry and Physics*, *15*(18), 10385–10397. https://doi.org/10.5194/acp-15-10385-2015

Kuttippurath, J., Lefèvre, F., Pommereau, J.-P., Roscoe, H. K., Goutail, F., Pazmiño, A., & Shanklin, J. D. (2013). Antarctic ozone loss in 1979–2010: First sign of ozone recovery. *Atmospheric Chemistry and Physics*, *13*(3), 1625–1635. https://doi.org/10.5194/acp-13-1625-2013

Laeng, A., Eckert, E., von Clarmann, T., Kiefer, M., Hubert, D., Stiller, G., et al. (2018). On the improved stability of the version 7 MIPAS ozone record. *Atmospheric Measurement Techniques*, *11*(8), 4693–4705. https://doi.org/10.5194/amt-11-4693-2018

Laeng, A., Grabowski, U., Von Clarmann, T., Stiller, G., Glatthor, N., Höpfner, M., et al. (2014). Validation of MIPAS IMK/IAA V5R_O3_224 ozone profiles. *Atmospheric Measurement Techniques*, *7*(11), 3971–3987. https://doi.org/10.5194/amt-7-3971-2014

Levy, H., Mahlman, J. D., Moxim, W. J., & Liu, S. C. (1985). Tropospheric ozone: The role of transport. *Journal of Geophysical Research*, *90*(D2), 3753–3772. https://doi.org/10.1029/JD090iD02p03753

López-Puertas, M., García-Comas, M., Funke, B., Gardini, A., Stiller, G. P., von Clarmann, T., et al. (2018). MIPAS observations of ozone in the middle atmosphere. *Atmospheric Measurement Techniques*, *11*(4), 2187–2212. https://doi.org/10.5194/amt-11-2187-2018

Lucke, R. L., Korwan, D. R., Bevilacqua, R. M., Hornstein, J. S., Shettle, E. P., Chen, D. T., et al. (1999). The polar ozone and aerosol measurement (POAM) III instrument and early validation results. *Journal of Geophysical Research*, *104*(D15), 18785–18799. https://doi.org/10.1029/2005JD006763

Marshall, B. T., Deaver, L. E., Thompson, R. E., Gordley, L. L., McHugh, M. J., Hervig, M. E., & Russell, J. M., III. (2010). Retrieval of temperature and pressure using broadband solar occultation: SOFIE approach and results. *Atmospheric Measurement Techniques*, *4*(5), 893–907. https://doi.org/10.5194/amtd-3-5743-2010

Marshall, B. T., Deaver, L. E., Thompson, R. E., Gordley, L. L., McHugh, M. J., Hervig, M. E., & Russell, J. M., III. (2011). Retrieval of temperature and pressure using broadband solar occultation: SOFIE approach and results. *Atmospheric Measurement Techniques*, *4*(5), 893–907. https://doi.org/10.5194/amt-4-893-2011

Mauldin, L. E., III, Zaun, N. H., McCormick, M. P., Jr., Guy, J. H., & Vaughn, W. R. (1985). Stratospheric aerosol and gas experiment II instrument: A functional description. *Optical Engineering*, *24*(2), 307–312. https://doi.org/10.1117/12.7973473

McCormick, M. P. (1987). SAGE II: An overview. *Advances in Space Research*, *7*(3), 219–226. https://doi.org/10.1016/0273-1177(87)90151-7

McCormick, M. P., Lei, L., Hill, M. T., Anderson, J., Querel, R., & Steinbrecht, W. (2020). Early results and validation of SAGE III-ISS ozone profile measurements from onboard the International Space Station. *Atmospheric Measurement Techniques*, *13*(3), 1287–1297. https://doi.org/10.5194/amt-13-1287-2020

McCormick, M. P., Zawodny, J. M., Veiga, R. E., Larsen, J. C., & Wang, P. H. (1989). An overview of SAGE I and II ozone measurements. *Planetary and Space Science*, *37*(12), 1567–1586. https://doi.org/10.1016/0032-0633(89)90146-3

McHugh, M., Magill, B., Walker, K. A., Boone, C. D., Bernath, P. F., & Russell, J. M., III. (2005). Comparison of atmospheric retrievals from ACE and HALOE. *Geophysical Research Letters*, *32*(15), L15S10. https://doi.org/10.1029/2005GL022403

Mitsuda, C., Suzuki, M., Iwata, Y., Manago, N., Naito, Y., Takahashi, C., et al. (2011). Current status of level 2 product of superconducting submillimeter-wave limb-emission sounder (SMILES). In *Sensors, systems, and next-generation satellites XV* (Vol. 8176, pp. 177–182). SPIE. https://doi.org/10.1117/12.898135

Müller, R., Grooß, J.-U., Lemmen, C., Heinze, D., Dameris, M., & Bodeker, G. (2008). Simple measures of ozone depletion in the polar stratosphere. *Atmospheric Chemistry and Physics*, *8*, 251–264. https://doi.org/10.5194/acp-8-251-2008

Natarajan, M., Damadeo, R., & Flittner, D. (2023). Solar occultation measurement of mesospheric ozone by SAGE III/ISS: Impact of variations along the line of sight caused by photochemistry. *Atmospheric Measurement Techniques*, *16*(1), 75–87. https://doi.org/10.5194/amt-16-75-2023

Natarajan, M., Deaver, L. E., Thompson, E., & Magill, B. (2005). Impact of twilight gradients on the retrieval of mesospheric ozone from HALOE. *Journal of Geophysical Research*, *110*(D13), D13305. https://doi.org/10.1029/2004JD005719

Newchurch, M. J., Allen, M., Gunson, M. R., Salawitch, R. J., Collins, G. B., Huston, K. H., et al. (1996). Stratospheric NO and NO_2 abundances from ATMOS solar-occultation measurements. *Geophysical Research Letters*, *23*(17), 2373–2376. https://doi.org/10.1029/96GL01196

Perliski, L. M., Solomon, S., & London, J. (1989). On the interpretation of seasonal variations of stratospheric ozone. *Planetary and Space Science*, *37*(12), 1527–1538. https://doi.org/10.1016/0032-0633(89)90143-8

Petelina, S. V., Llewellyn, E. J., Walker, K. A., Degenstein, D. A., Boone, C. D., Bernath, P. F., et al. (2005). Validation of ACE-FTS stratospheric ozone profiles against Odin/OSIRIS measurements. *Geophysical Research Letters*, *32*(15). https://doi.org/10.1029/2005GL022377

Randel, W. J., Garcia, R., & Wu, F. (2008). Dynamical balances and tropical stratospheric upwelling. *Journal of the Atmospheric Sciences*, *65*(11), 3584–3595. https://doi.org/10.1175/2008JAS2756.1

Riese, M., Ploeger, F., Rap, A., Vogel, B., Konopka, P., Dameris, M., & Forster, P. (2012). Impact of uncertainties in atmospheric mixing on simulated UTLS composition and related radiative effects. *Journal of Geophysical Research*, *117*, 16305. https://doi.org/10.1029/2012JD017751

Russell, J. M., III, Bailey, S. M., Gordley, L. L., Rusch, D. W., Horányi, M., Hervig, M. E., et al. (2009). The Aeronomy of Ice in the Mesosphere (AIM) mission: Overview and early science results. *Journal of Atmospheric and Solar-Terrestrial Physics*, *71*(3–4), 289–299. https://doi.org/10.1016/j.jastp.2008.08.011

Russell, J. M., III, & Drayson, S. R. (1972). The inference of atmospheric ozone using satellite horizon measurements in the 1042 cm^{-1} band. *Journal of the Atmospheric Sciences*, *29*(2), 376–390. https://doi.org/10.1175/1520-0469(1972)029<0376:TIOAOU>2.0.CO;2

Russell, J. M., III, Farmer, C. B., Rinsland, C. P., Zander, R., Froidevaux, L., Toon, G. C., et al. (1988). Measurements of odd nitrogen compounds in the stratosphere by the ATMOS experiment on Spacelab 3. *Journal of Geophysical Research*, *93*(D2), 1718–1736. https://doi.org/10.1029/jd093id02p01718

Russell, J. M., III, Gordley, L. L., Park, J. H., Drayson, S. R., Hesketh, W. D., Cicerone, R. J., et al. (1993). The halogen occultation experiment. *Journal of Geophysical Research*, *98*(D6), 10777–10797. https://doi.org/10.1029/93JD00799

Russell, J. M., III, Mlynczak, M. G., Gordley, L. L., Tansock, J. J., Jr., & Esplin, R. W. (1999). Overview of the SABER experiment and preliminary calibration results. In *Optical spectroscopic techniques and instrumentation for atmospheric and space research III* (Vol. 3756, pp. 277–288). SPIE. https://doi.org/10.1117/12.366382

Safieddine, S., Bouillon, M., Paracho, A. C., Jumelet, J., Tencé, F., Pazmino, A., et al. (2020). Antarctic ozone enhancement during the 2019 sudden stratospheric warming event. *Geophysical Research Letters*, *47*(14), e2020GL087810. https://doi.org/10.1029/2020gl087810

SAGE III ATBD Team. (2002). SAGE III algorithm theoretical basis document (ATBD) solar and lunar algorithm, LaRC 475-00-109, version 2.1. Retrieved from https://eospso.gsfc.nasa.gov/sites/default/files/atbd/atbd-sage-solar-lunar.pdf

Salby, M., Titova, E., & Deschamps, L. (2011). Rebound of Antarctic ozone. *Geophysical Research Letters*, *38*, L09702. https://doi.org/10.1029/2011GL047266

Serdyuchenko, A., Gorshelev, V., Weber, M., Chehade, W., & Burrows, J. P. (2014). High spectral resolution ozone absorption cross-sections–Part 2: Temperature dependence. *Atmospheric Measurement Techniques*, *7*(2), 625–636. https://doi.org/10.5194/amt-7-625-2014

Sheese, P. E., Walker, K. A., Boone, C. D., Bernath, P. F., Froidevaux, L., Funke, B., et al. (2017). ACE-FTS ozone, water vapour, nitrous oxide, nitric acid, and carbon monoxide profile comparisons with MIPAS and MLS. *Journal of Quantitative Spectroscopy and Radiative Transfer*, *186*, 63–80.

Sheese, P. E., Walker, K. A., Boone, C. D., Bourassa, A. E., Degenstein, D. A., Froidevaux, L., et al. (2022). Assessment of the quality of ACE-FTS stratospheric ozone data. *Atmospheric Measurement Techniques*, *15*(5), 1233–1249. https://doi.org/10.5194/amt-15-1233-2022

Sinnhuber, B. M., Chipperfield, M. P., Davies, S., Burrows, J. P., Eichmann, K. U., Weber, M., et al. (2000). Large loss of total ozone during the Arctic winter of 1999/2000. *Geophysical Research Letters*, *27*, 3473–3476. https://doi.org/10.1029/2000GL011772

Smith, A. K., Harvey, V. L., Mlynczak, M. G., Funke, B., García-Comas, M., Hervig, M., et al. (2013). Satellite observations of ozone in the upper mesosphere. *Journal of Geophysical Research: Atmospheres*, *118*(11), 5803–5821. https://doi.org/10.1002/jgrd.50445

Smith, A. K., López-Puertas, M., García-Comas, M., & Tukiainen, S. (2009). SABER observations of mesospheric ozone during NH late winter 2002–2009. *Geophysical Research Letters*, *36*(23), L23804. https://doi.org/10.1029/2009GL040942

Smith, A. K., & Marsh, D. R. (2005). Processes that account for the ozone maximum at the mesopause. *Journal of Geophysical Research*, *110*(D23), D23305. https://doi.org/10.1029/2005JD006298

Smith, A. K., Marsh, D. R., Mlynczak, M. G., Russell, J. M., & Mast, J. C. (2011). SABER observations of daytime atomic oxygen and ozone variability in the mesosphere. In *Aeronomy of the Earth's atmosphere and ionosphere* (pp. 75–82). Springer. https://doi.org/10.1007/978-94-007-0326-1_5

Smith, A. K., Marsh, D. R., Russell, J. M., III, Mlynczak, M. G., Martin-Torres, F. J., & Kyrölä, E. (2008). Satellite observations of high nighttime ozone at the equatorial mesopause. *Journal of Geophysical Research*, *13*(D17), D17312. https://doi.org/10.1029/2008JD010066

SOFIE Science Team. (2007). The SOFIE V 1.3 temperature (Temperature), and ozone (O_3) products [Dataset]. SOFIE Science Team. Retrieved from http://sofie.gats-inc.com/getdata

Solomon, S., Garcia, R. R., & Stordal, F. (1985). Transport processes and ozone perturbations. *Journal of Geophysical Research*, *90*(D7), 12981–12989. https://doi.org/10.1029/JD090iD07p12981

Solomon, S., Haskins, J., Ivy, D. J., & Min, F. (2014). Fundamental differences between Arctic and Antarctic ozone depletion. *Proceedings of the National Academy of Sciences of the United States of America*, *111*(17), 6220–6225. https://doi.org/10.1073/pnas.1319307111

Solomon, S., Ivy, D. J., Kinnison, D., Mills, M. J., Neely, R. R., & Schmidt, A. (2016). Emergence of healing in the Antarctic ozone layer. *Science*, *353*, 269–274. https://doi.org/10.1126/science.aae0061

Steck, T., Von Clarmann, T., Fischer, H., Funke, B., Glatthor, N., Grabowski, U., et al. (2007). Bias determination and precision validation of ozone profiles from MIPAS-Envisat retrieved with the IMK-IAA processor. *Atmospheric Chemistry and Physics*, *7*(13), 3639–3662. https://doi.org/10.5194/acp-7-3639-2007

Stiller, G. P., Kiefer, M., Eckert, E., Von Clarmann, T., Kellmann, S., García-Comas, M., et al. (2012). Validation of MIPAS IMK/IAA temperature, water vapor, and ozone profiles with MOHAVE-2009 campaign measurements. *Atmospheric Measurement Techniques*, *5*(2), 289–320. https://doi.org/10.5194/amt-5-289-2012

Stolarski, R., Bojkov, R., Bishop, L., Zerefos, C., Staehelin, J., & Zawodny, J. (1992). Measured trends in stratospheric ozone. *Science*, *256*(5055), 342–349. https://doi.org/10.1126/science.256.5055.342

Stolarski, R. S., Bloomfield, P., McPeters, R. D., & Herman, J. R. (1991). Total ozone trends deduced from Nimbus 7 TOMS data. *Geophysical Research Letters*, *18*(6), 1015–1018. https://doi.org/10.1029/91GL01302

Takahashi, C., Suzuki, M., Mitsuda, C., Ochiai, S., Manago, N., Hayashi, H., et al. (2011). Capability for ozone high-precision retrieval on JEM/SMILES observation. *Advances in Space Research*, *48*(6), 1076–1085. https://doi.org/10.1016/j.asr.2011.04.038

Tritscher, I., Pitts, M. C., Poole, L. R., Alexander, S. P., Cairo, F., Chipperfield, M. P., et al. (2021). Polar stratospheric clouds: Satellite observations, processes, and role in ozone depletion. *Reviews of Geophysics*, *59*(2), e2020RG000702. https://doi.org/10.1029/2020RG000702

Tweedy, O. V., Limpasuvan, V., Orsolini, Y. J., Smith, A. K., Garcia, R. R., Kinnison, D., et al. (2013). Nighttime secondary ozone layer during major stratospheric sudden warmings in specified-dynamics WACCM. *Journal of Geophysical Research: Atmospheres*, *118*(15), 8346–8358. https://doi.org/10.1002/jgrd.50651

von der Gathen, P., Kivi, R., Wohltmann, I., Salawitch, R. J., & Rex, M. (2021). Climate change favours large seasonal loss of Arctic ozone. *Nature Communications*, *12*, 3886. https://doi.org/10.1038/s41467-021-24089-6

von Clarmann, T. (2006). Validation of remotely sensed profiles of atmospheric state variables: Strategies and terminology. *Atmospheric Chemistry and Physics*, *6*(12), 4311–4320. https://doi.org/10.5194/acp-6-4311-2006

Walker, K. A., Randall, C. E., Trepte, C. R., Boone, C. D., & Bernath, P. F. (2005). Initial validation comparisons for the atmospheric chemistry experiment (ACE-FTS). *Geophysical Research Letters*, *32*(16), L16S04. https://doi.org/10.1029/2005GL022388

Waters, J. W., Froidevaux, L., Harwood, R. S., Jarnot, R. F., Pickett, H. M., Read, W. G., et al. (2006). The Earth observing system microwave limb sounder (EOS MLS) on the Aura satellite. *IEEE Transactions on Geoscience and Remote Sensing*, *44*(5), 1075–1092. https://doi.org/10.1109/TGRS.2006.873771

World Meteorological Organization (WMO). (2022). *Executive summary. Scientific assessment of ozone depletion: 2022, GAW report no. 278* (p. 56). WMO.